ARNOLD DIFFUSION IN THE ELLIPTIC HILL FOUR-BODY PROBLEM: GEOMETRIC METHOD AND NUMERICAL VERIFICATION

JAIME BURGOS-GARCÍA, MARIAN GIDEA, AND CLAUDIO SIERPE

ABSTRACT. We present a mechanism for Arnold diffusion in energy in a model of the elliptic Hill four-body problem. Our model is expressed as a small perturbation of the circular Hill four-body problem, with the small parameter being the eccentricity of the orbits of the primaries. The mechanism relies on the existence of two normally hyperbolic invariant manifolds (NHIM's), and on the corresponding homoclinic and heteroclinic connections. The dynamics along homoclinic/heteroclinic orbits is encoded via scattering maps, which we compute numerically. Having several scattering maps, at each point we select the scattering map that gives the largest gain in energy or the scattering map that gives the smallest loss in energy. Using Birkhoff's Ergodic Theorem we show that there are pseudo-orbits generated by the selected scattering maps along which, on average, the energy grows by an amount independent of the small parameter. A shadowing lemma yields the existence of diffusing orbits.

1. Introduction

1.1. Overview of results. We consider the planar elliptic restricted four-body problem (ER4BP), describing the dynamics of a massless body under the gravitational influence of three massive bodies (primaries) of masses $m_1 > m_2 > m_3$ forming an equilateral central configuration, where each primary moves on an elliptic orbit about the common center of mass. This represents a homographic solution of the general three-body problem. We derive the elliptic Hill four-body problem (EH4BP), which is an approximation of the ER4BP describing the dynamics of the infinitesimal body in a neighborhood of the smaller body, in the limit case when $m_3 \to 0$ and m_1, m_2 are sent to infinity. The EH4BP can be written as a perturbation of the circular Hill four-body problem (CH4BP), with the eccentricity ϵ of the

²⁰²⁰ Mathematics Subject Classification. Primary: 70F10, 70H08, 37J40; Secondary: 70F15, 37E40.

Key words and phrases. Elliptic four-body problem, Hill's problem, normally hyperbolic invariant manifolds, Arnold diffusion.

The work of M.G. was partially supported by NSF grant DMS-2307718. The work of C.S. was supported by ANID-Chile through Beca de Doctorado Nacional, folio 21191713. Part of the work was carried out while C.S. was visiting Yeshiva University during 2022-2023.

elliptic orbits being the small parameter. While for some orbits the effect of the perturbation may average out, for other orbits it may accumulate in the long run. We show that the EH4BP exhibits Arnold diffusion, in the sense that there exist orbits of the infinitesimal body that undergo significant changes over time. In particular, the energy along these orbits increases by O(1) with respect to the perturbation parameter ϵ .

A motivation for this work is the system consisting of Sun, Jupiter, the Trojan asteroid (624) Hektor, and its moonlet Skamandrios, which can be modeled by the EH4BP. Hektor is located close to the Lagrangian point L_4 of the Sun-Jupiter system. The motion of Skamandrios exhibits various resonances, so a small perturbation could potentially lead to ejection of the moonlet or to collision with the asteroid [MDCR⁺14]. There is a theoretical possibility that Arnold diffusion may lead to such scenarios.

1.2. **Methodology.** Our arguments for Arnold diffusion rely on geometric methods and numerical verifications.

The geometric method is concerned with identifying the geometric objects that organize the dynamics for the unperturbed system, and computing the effect of the perturbation on these objects.

For the unperturbed problem, corresponding to the CH4BP, we find 4 equilibrium points: L_1 , L_2 , of center-saddle linear stability type, and L_3 , L_4 , of center-center type. We focus on the dynamics near L_1 , L_2 . For a range of energies slightly above that of L_1 , L_2 , we find families of Lyapunov periodic orbits around these points. Each family forms a normally hyperbolic invariant manifold (NHIM), which is an annulus that can be parametrized via symplectic action-angle coordinates. The NHIM's posses stable and unstable manifolds. For these energies, the motion of the massless body is confined to an inner region around m_3 connected to an outer region opening towards m_1 , m_2 . The two regions are separated by two 'bottlenecks' where the Lyapunov orbits near L_1 , L_2 lie. There exist transverse homoclinic and heteroclinic connections between the two NHIM's within both the inner region and the outer region. Each homoclinic orbit is asymptotic in both forward and backwards time to the same Lyapunov orbit, and each heteroclinic orbit is asymptotic in forward and backwards time to two Lyapunov orbits – one near L_1 and the other near L_2 – of the same energy. We can encode the asymptotic behavior of homoclinic/heteroclinic orbits via the scattering map – a geometrically defined map acting on the NHIM's. It turns out that, when expressed in action-angle coordinates, the unperturbed scattering map preserves the action and shifts the angle coordinate.

We then consider the effect of the perturbations on the NHIM's and on the transverse homoclinic/heteroclinic orbits. For small perturbations, the NHIM's survive while being slightly deformed, due to the standard normally hyperbolicity theory. The transverse homoclinic/heteroclinic orbits also survive, due to the robustness of transversality. However the perturbed scattering map can increase or decrease the action coordinate. Using deformation theory, one can compute the perturbed scattering map as an expansion in terms of the perturbation parameter: the zero-th order term in the expansion is the unperturbed scattering map, and the first order term is given by a Hamiltonian function in the action-angle variables. This Hamiltonian can be explicitly computed via Melnikov theory in terms of improper, convergent integrals of the perturbation along homoclinic/heteroclinic orbits of the unperturbed system. Moreover, these integrals converge exponentially fast, which allows for their efficient numerical computation. Through the computation of the perturbed scattering map, we can identify regions where a scattering map increases the action coordinate by $O(\epsilon)$, as well as regions where a scattering map decreases the action coordinate by $O(\epsilon)$. In this paper, we make use of several scattering maps. On the domains where the scattering maps increase the action, we select the scattering map that yields the largest growth in action, and on the domains where the scattering maps decrease the action, we select the scattering map that yields the smallest decay in action. We then apply Birkhoff's Ergodic Theorem to show that there exist pseudo-orbits generated by the selected scattering maps along which the action grows on average by O(1). Finally, a shadowing lemma shows that there are true orbits along which the action grows by O(1).

When the action increases, the corresponding Lyapunov periodic orbits get bigger, and their stable/unstable manifolds in the inner region pass closer to m_3 . At the same time, the 'bottlenecks' around L_1 , L_2 get wider, and orbits can escape more easily from the inner region to the outer region. In the context of the Sun-Jupiter-Hektor system, it is possible that, in the long run, Arnold diffusion can push the moonlet Skamandrios towards collision with Hektor, or, on the contrary, to escape from Hektor's capture.

While our numerical calculations are not validated via computer assisted proofs, they are sufficiently accurate by numerical analysis standards. A rigorous numerical verification can be done using the CAPD library [KMWZ21].

The novel aspects of this work can be summarized as follows:

- We derive the Hamiltonian for the EH4BP and write it is as a perturbation of the CH4BP.
- We show the existence of Arnold diffusion for the EH4BP, in a model with realistic parameters for the masses of the bodies and for the energy levels.
- We describe an argument for diffusion based on several scattering maps, where at each step we select either the scattering map that gives the largest energy growth or the one that gives the smallest energy loss, so on the average we keep growing energy.
- We compare two diffusion mechanisms via homoclinic and via heteroclinic orbits.
- We provide a complete chart of diffusion pathways in terms of the level sets of the Hamiltonians that generate the scattering maps.

1.3. Related works. The Arnold Diffusion problem [Arn64] asserts that integrable Hamiltonian systems subject to small, generic perturbations, have diffusing orbits along which the action coordinate changes by an amount independent of the size of the perturbation. While Arnold illustrated this phenomenon on a simple model consisting of a rotator and a pendulum plus a small time-dependent perturbation of a special type, he conjectured "I believe that the mechanism of transition chain that guarantees that nonstability in our example is applicable to the general case (for example, to the problem of three bodies)".

Despite its long history, there are few results on proving Arnold diffusion in celestial mechanics, particularly with realistic parameters (e.g., for the masses of the bodies, or for the energy levels). Some works prove Arnold diffusion in realistic models of the restricted three-body problem by combining analytical methods with numerical computations. The paper [FGKR16] shows that diffusion along mean motion resonances in the Sun-Jupiter system can be used to explain the Kirkwood gaps in the main asteroid belt. The paper [CGDlL17] shows the existence of orbits that exhibit Arnold diffusion in energy for the Sun-Jupiter system at energy levels close to that of the comet Oterma. A computer assisted proof for Arnold diffusion in energy for the Neptune-Triton system is given in [CG23]; moreover, this paper shows that the energy of diffusing orbits evolves according to a Brownian motion with drift. Numerical evidence for Arnold diffusion in the dynamics of Jupiter's Trojan asteroids is provided in [RG06], by the means of the Frequency Map Analysis [Las90].

There are some purely analytical proofs of Arnold diffusion in celestial mechanics models. These include [DKdlRS19] where, in the case of the planar elliptic restricted three-body problem, for mass ratio and eccentricities of the primaries sufficiently small, they construct orbits with large drift in angular momentum. This result is extended for arbitrary masses in [GPS23]. The paper [CFG22] proves Arnold's conjecture in a planetary spatial 4-body problem as well as in the corresponding hierarchical problem (where the bodies are increasingly separated); in particular, they show that one of the planet may change inclination in a random fashion, and, moreover, it can flip from a prograde nearly horizontal orbit to a retrograde one.

In the present paper, we use analytical methods and numerical verifications to show Arnold diffusion in an elliptic Hill four-body problem modeling the dynamics of the moonlet Skamandrios relative to the Sun-Jupiter-Hektor system, for realistic values of the masses and energies. In this model, the diffusion mechanism can affect the orbit of the moonlet dramatically, so that it can pass closer and closer to the asteroid, or it can escape from the asteroid's capture. A model for this system based on the circular Hill four-body problem is derived in [BGG15], and further studied in [BG16, BGBFP22]. The paper [BGCG⁺20] develops a model that takes into account the highly oblate shape of Hektor, and derives a circular Hill four-body problem in this

case. In a follow-up paper [BGL23], collision orbits are studied via McGehee regularization. The geometric approach that we use in the present paper has the advantage that it can be adapted to incorporate additional realistic effects, such as the oblateness of the asteroid. We can also include the effect of inclination of the orbits of the asteroid and of the moonlet, as in [DGR16], or the effect of dissipation, as in [AGMS23].

The methodology to prove diffusion in our model is similar to that in [CGDlL17]. The main tool that we use is the scattering map. This was used in [DdlLS06a] to prove Arnold diffusion in a priori unstable Hamiltonian systems; see also the related papers [DdlLS00, DdlLS06b]. The geometric properties of the scattering map have been studied in [DdlLS08]. A general mechanism of diffusion that relies mostly on the scattering map, and uses only the Poincaré recurrence of the inner dynamics (which is automatically satisfied in Hamiltonian systems over regions of bounded measure) was developed in [GdlLMS20] (see also [GdlLMS19]). This mechanism applies only in the case when the unperturbed scattering map is the identity. In the present paper, we introduce a new mechanism of diffusion based on several scattering maps. Unlike in [GdlLMS20], the unperturbed scattering map is a shift in the angle variable rather than the identity. Also, unlike in [CGDlL17], where for each point in the NHIM we can always select a scattering map that increases the energy, in the present model, besides domains where the scattering maps increase the energy there are also domains where they decrease the energy. We use Birkhoff's Ergodic Theorem to show that we can intertwine the application of the scattering maps so that, on average, we can grow the energy. The idea of estimating the average growth of energy along orbits also appears in [GdlL17].

An important quality of the scattering map that we explore in this paper is that it can be computed explicitly, either analytically, via perturbation theory, or numerically [DdlLS06a, DGR16]. In the perturbative case, the perturbed scattering map can be expanded in powers of the perturbation parameter, such that the zero-th order term in the expansion is the unperturbed scattering map, and the first order term is given by a Hamiltonian function on the NHIM. These level sets can be use to detect the fastest pathways for diffusing orbits [DS18, DS17, DGR]. In the present work, we perform a direct computation of the level sets of the Hamiltonians generating the scattering maps associated to homoclinic as well as to heteroclinic connections, and discuss their role in diffusion.

1.4. Structure of the paper. In Section 2 we describe the ER4BP. In Section 3 we derive the Hill approximation for the ER4BP, and we express the Hamiltonian of the EH4BP as a perturbation of the CH4BP. In Section 4 we describe the geometric objects that organize the dynamics in the CH4BP: equilibrium points, Lyapunov periodic orbits, and their stable and unstable manifolds. We also provide numerical evidence for the existence of

homoclinic and heteroclinic connections. In Section 5 we provide a geometric method to show the existence of Arnold diffusion, and then in Section 6 we implement it numerically in the case of the EH4BP.

2. The elliptic restricted four body problem

Consider a massless particle that moves on the same plane of three massive bodies, called primaries, without affecting their motion. The equations for the massless particle in a (X,Y) inertial coordinate system with origin at the center of mass of the system are given by

(1)
$$\frac{d^2X}{dt^2} = -G\sum_{i=1}^3 \frac{m_i(X - X_i)}{\rho_i^3}, \quad \frac{d^2Y}{dt^2} = -G\sum_{i=1}^3 \frac{m_i(X - X_i)}{\rho_i^3},$$

where (X_i, Y_i) are the positions of the three primaries, ρ_i is the distance between the massless particle and each primary for i = 1, 2, 3, and G denotes the gravitational constant. Using the complex coordinate Z = X + iY we can write the equations (1) in the following form

(2)
$$\frac{d^2Z}{dt^2} = -G\sum_{i=1}^3 \frac{m_i(Z - Z_i)}{\rho_i^3},$$

with $\rho_i = |Z - Z_i|$. The positions of the primaries can be considered as solutions of the three-body problem such as the Euler solution [ML99], the eight-shaped solution [LB22], or the Lagrange solution to produce different kinds of restricted four-body problems. Some authors have considered elliptical motions for the primaries which are not actual solutions of the three-body to generate other kinds of elliptic restricted four-body problems [LG18, CPT22].

The restricted four-body problem considering the Lagrangian configuration has been studied recently by several authors for the case when the primaries move in circular orbits. See for instance, [BGD13b, BGD13a, BGLJ19] and references therein. However, there are few studies of the elliptic case [CN19, AP20] where the equations of motion were obtained for special values of the masses. Since the Lagrange solution exists for all the physical values of the masses and we are interested in the case when one primary is too small compared with the remaining two, we provide a full discussion of the problem considering the elliptic case to obtain the equations of motion of the elliptic restricted four-body problem, hereafter referred as ER4BP.

We start considering solutions of the planar three-body problem (in complex notation) of the form $q_i(t) = \phi(t)a_i$ where each a_i is a complex number and $\phi(t)$ is a time-dependent complex-valued function. It is well known that the substitution of this expression into the equations of the three-body

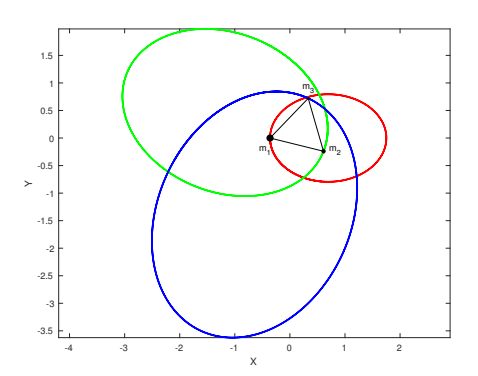


FIGURE 1. The solution of the Lagrangian central configuration of the three body problem with $m_1 = 0.6$, $m_2 = 0.3$, $m_3 = 0.1$ and $\epsilon = 0.13$.

problem gives rise to the equations [Mey09]:

(3)
$$\frac{d^2\phi}{dt^2} = -\frac{\lambda\phi}{|\phi|^3},$$

(4)
$$\frac{\partial U}{\partial a}(a) + \lambda \frac{\partial I}{\partial a}(a) = 0,$$

where $q=(q_1,q_2,q_3)$, $a=(a_1,a_2,a_3)$, U is the potential of the three-body problem and $I=\frac{1}{2}\left(m_1|q_1|^2+m_2|q_2|^2+m_3|q_3^2|\right)$ is the moment of inertia of the system. The solutions of (4) give a central configurations of the three-body problem, and the equation (3) is a two-dimensional Kepler problem. The solutions of the equation (4) are the celebrated Euler (collinear) and Lagrange (equilateral) configurations. See Fig. 1. Moreover, the Lagrangian configuration was studied in [BGCG⁺20] when the masses are considered as oblate bodies and the main conclusion is that the equilateral shape of the configuration deforms into an isosceles or a scalene triangle depending on the oblateness of the bodies.

For the equilateral configuration the distances between the three primaries $\rho_{ij} = ||q_i - q_j||$ satisfy

$$\rho_{12} = \rho_{23} = \rho_{31} = \left(\frac{GM}{\lambda}\right)^{-1/3}$$

where λ is a scale factor that fixes the size of the system and $M = m_1 + m_2 + m_3$. For the elliptic solutions of (3) the function $\phi(t)$ can be written in polar coordinates $\phi(t) = re^{if}$, where r and f satisfy the two dimensional

Kepler problem

(5)
$$\frac{dr}{dt} - r \left(\frac{df}{dt}\right)^2 = -\frac{\lambda}{r^2},$$

$$(6) r^2 \frac{df}{dt} = c,$$

and they are related by

(7)
$$r = \frac{c^2/\lambda}{1 + \epsilon \cos(f)}.$$

The constant c is the magnitude of the angular momentum, ϵ denotes the eccentricity, and f is the true anomaly.

Now, to consider the positions of the primaries fixed, we introduce the so-called pulsating coordinates

$$(8) Z = re^{if}z,$$

where we can apply the chain rule to obtain the expressions

$$\frac{dz}{dt} = \frac{dz}{df}\frac{df}{dt}, \quad \frac{d^2z}{dt^2} = \frac{dz}{df}\frac{d^2f}{dt^2} + \frac{d^2z}{df^2}\left(\frac{df}{dt}\right)^2,$$

which are necessary to compute the second derivative in the expression (8). A straightforward computation shows that the second derivative of Z is given by

$$\frac{d^2Z}{dt^2}e^{-if} = r\left(\frac{df}{dt}\right)^2\left(\frac{d^2z}{df^2} + 2i\frac{dz}{df}\right) + z\left(\frac{dr}{dt} - r\left(\frac{df}{dt}\right)^2\right) + \left(\frac{dz}{df} + iz\right)\left(r^2\frac{d^2f}{dt^2} + 2\frac{dr}{dt}\frac{df}{dt}\right).$$

The second term on the right side of the above equation corresponds to the equation (5), and the third term are equal to zero because the term

$$r^2 \frac{d^2 f}{dt^2} + 2 \frac{dr}{dt} \frac{df}{dt}$$

is the derivative of the expression (6). Therefore, the left side of the equation (2) becomes

(9)
$$\frac{d^2Z}{dt^2} = e^{if} \left(r \left(\frac{df}{dt} \right)^2 \left(\frac{d^2z}{df^2} + 2i\frac{dz}{df} \right) - z\frac{\lambda}{r^2} \right).$$

On the other hand, using the expression (8), the right-side of (2) becomes

(10)
$$-G\sum_{i=1}^{3} \frac{m_i(Z-Z_i)}{\rho_i^3} = -\frac{Ge^{if}}{r^2} \sum_{i=1}^{3} \frac{m_i(z-z_i)}{|z-z_i|^3}.$$

If we define $\mu_i = m_i/M$, where M is the total mass of the system, the equation (2) in pulsating coordinates is given by the expression:

(11)
$$r \left(\frac{df}{dt}\right)^2 \left(\frac{d^2z}{df^2} + 2i\frac{dz}{df}\right) = z\frac{\lambda}{r^2} - \frac{GM}{r^2} \sum_{i=1}^3 \frac{\mu_i(z - z_i)}{|z - z_i|^3}.$$

From equations (7) and (6) we obtain

$$\frac{1}{r^2} = \frac{r\left(\frac{df}{dt}\right)^2}{\lambda(1 + \epsilon\cos(f))},$$

so the equation (11) becomes

$$r\left(\frac{df}{dt}\right)^2 \left(\frac{d^2z}{df^2} + 2i\frac{dz}{df}\right) = \frac{r\left(\frac{df}{dt}\right)^2}{1 + \epsilon\cos(f)} \left(z - \frac{GM}{\lambda}\sum_{i=1}^3 \frac{\mu_i(z - z_i)}{|z - z_i|^3}\right).$$

We recall that the distances between the primaries are given by $\rho_{ij} = \left(\frac{GM}{\lambda}\right)^{-1/3}$ so, in order to fix the length of the triangle equal to 1, we choose $\lambda = GM$. Dividing the above equation by $r\left(\frac{df}{dt}\right)^2$ we obtain

(12)
$$\frac{d^2z}{df^2} + 2i\frac{dz}{df} = \frac{1}{1 + \epsilon \cos(f)} \left(z - \sum_{i=1}^3 \frac{\mu_i(z - z_i)}{|z - z_i|^3} \right).$$

In the new coordinates, the positions z_i are the solutions of equation (4) and consequently, the positions are constant and the coordinates are given by the same expressions used in the circular version of the ER4BP:

$$x_1 = \frac{-|K|\sqrt{m_2^2 + m_2m_3 + m_3^2}}{K} \qquad y_1 = 0$$

$$x_2 = \frac{|K|[(m_2 - m_3)m_3 + m_1(2m_2 + m_3)]}{2K\sqrt{m_2^2 + m_2m_3 + m_3^2}} \qquad y_2 = \frac{-\sqrt{3}m_3}{2m_2^{3/2}}\sqrt{\frac{m_2^3}{m_2^2 + m_2m_3 + m_3^2}}$$

$$x_3 = \frac{|K|}{2\sqrt{m_2^2 + m_2m_3 + m_3^2}} \qquad y_3 = \frac{\sqrt{3}}{2\sqrt{m_2}}\sqrt{\frac{m_2^3}{m_2^2 + m_2m_3 + m_3^2}},$$

where $K = m_2(m_3 - m_2) + m_1(m_2 + 2m_3)$, and we have reconsidered the mass ratios μ_i as m_i in such a way that they satisfy $m_1 + m_2 + m_3 = 1$.

If we denote by $\dot{z} = \frac{dz}{df}$ and separate the real and imaginary parts of z = x + iy in (12), we obtain the equations in Cartesian coordinates

(13)
$$\ddot{x} - 2\dot{y} = \Omega_x, \\ \ddot{y} + 2\dot{x} = \Omega_y,$$

where

$$\Omega(x, y; m_1, m_2, m_3) = \frac{1}{1 + \epsilon \cos(f)} \left(\frac{1}{2} (x^2 + y^2) + \sum_{i=1}^{3} \frac{m_i}{r_i} \right),$$

and $r_i = \sqrt{(x-x_i)^2 + (y-y_i)^2}$, for i = 1, 2, 3. Making the transformation $\dot{x} = p_x + y$, $\dot{y} = p_y - x$, we obtain that the equations (13) are equivalent to the equations given by the Hamiltonian (14)

$$H = \frac{1}{2}(p_x^2 + p_y^2) + yp_x - xp_y + \frac{1}{2}(x^2 + y^2) - \frac{1}{1 + \epsilon \cos(f)} \left(\frac{1}{2}(x^2 + y^2) + \sum_{i=1}^{3} \frac{m_i}{r_i} \right).$$

Remark 2.1. Since a planar homographic solution of the general N-body problem is defined as $q_i(t) = r(t)e^{i\theta(t)}a_i$ where the a_i 's describe a central configuration, and r(t) and $\theta(t)$ satisfy the equations (5) and (6), the performed construction can be easily extended to generate elliptic restricted problems for N > 3 primaries moving in homographic solutions.

3. The limit case and equations of motion

In this section we study the limit case when $m_3 \to 0$ in the Hamiltonian of the ER4BP. For our purposes it is sufficient to consider small values of the eccentricity, however, the procedure can be easily extended for all values of eccentricity. Expanding the expression $1/(1 + \epsilon \cos(f))$ in terms of the eccentricity in a neighborhood of $\epsilon = 0$ we have

(15)
$$\frac{1}{1 + \epsilon \cos(f)} = 1 - \epsilon \cos(f) + \mathcal{O}(\epsilon^2).$$

Therefore the Hamiltonian (14) becomes

(16)
$$H_{ER4BP} = H_{CR4BP} + \epsilon \cos(f) \left(\frac{1}{2} (x^2 + y^2) + \sum_{i=1}^{3} \frac{m_i}{r_i} \right) + \mathcal{O}(\epsilon^2),$$

where H_{CR4BP} is the Hamiltonian of the circular restricted four body problem.

Theorem 3.1. Let H_{CH4BP} be the Hamiltonian of the circular Hill four-body problem, given by

(17)
$$H_{CH4BP} = \frac{1}{2}(p_x^2 + p_y^2) + yp_x - xp_y - U(x, y),$$

with

(18)
$$U(x,y) = -\frac{1}{8}x^2 + \frac{3\sqrt{3}}{4}(1-2\mu)xy + \frac{5}{8}y^2 + \frac{1}{\sqrt{x^2+y^2}}$$

being the gravitational potential relative to the co-rotating frame, $m_1 = 1 - \mu$ and $m_2 = \mu$.

Then, for small values of the eccentricity ϵ , and after the conformally symplectic scaling

$$(x, y, p_x, p_y) \to m_3^{1/3}(x, y, p_x, p_y),$$

the limiting Hamiltonian (16) as $m_3 \rightarrow 0$ is

(19)
$$H_{EH4BP} = H_{CH4BP} + \epsilon \cos(f) \left(\frac{1}{2} (x^2 + y^2) + U(x, y) \right) + O(\epsilon^2).$$

The system associated to H_{EH4BP} yields an approximation of the motion of the infinitesimal mass in an $O(m_3^{1/3})$ -neighborhood of m_3 , and will be referred to as the Elliptic Hill's Four-Body Problem (EH4BP).

Proof. If we ignore the higher order terms in the Hamiltonian (16) we can write it as

(20)
$$H = H_{CH4BP} + \epsilon \cos(f)H_1.$$

The Hill approximation for the Hamiltonian H_{CH4BP} was already carried out in [BGG15], therefore it will be enough to work with H_1 . First, we perform the change of coordinates $x \to x + x_3$, $y \to y + y_3$, $p_x \to p_x - y_3$, $p_y \to p_y + x_3$, therefore in these new coordinates the term (20) becomes

$$H_1 = \frac{1}{2}(x^2 + y^2) + x_3x + y_3y + \sum_{i=1}^{3} \frac{m_i}{\bar{r}_i},$$

where we have omitted the constant term $\frac{1}{2}(x_3^2+y_3^2)$ and $\bar{r}_i^2=(x+x_3-x_i)^2+(y+y_3-y_i)^2:=(x+\bar{x}_i)^2+(y+\bar{y}_i)^2$, for i=1,2,3. We expand the terms $\frac{1}{\bar{r}_1}$ and $\frac{1}{\bar{r}_2}$ in Taylor series around the new origin of coordinates; if we ignore the constant terms we obtain the following expressions

$$f^{1} := \frac{1}{\bar{r}_{1}} = \sum_{k \ge 1} P_{k}^{1}(x, y),$$
$$f^{2} := \frac{1}{\bar{r}_{2}} = \sum_{k \ge 1} P_{k}^{2}(x, y),$$

where $P_k^j(x,y)$ is a homogenous polynomial of degree k for j=1,2. We perform the conformally symplectic scaling $x \to m_3^{1/3} x$, $y \to m_3^{1/3} y$, $p_x \to m_3^{1/3} p_x$, $p_y \to m_3^{1/3} p_y$ with multiplier $m_3^{-2/3}$, obtaining

(21)
$$H_{1} = \frac{1}{2}(x^{2} + y^{2}) + \frac{1}{\sqrt{x^{2} + y^{2}}} + m_{3}^{-1/3}(x_{3}x + y_{3}y + P_{1}^{1} + P_{1}^{2}) + \sum_{k \geq 2} m_{3}^{\frac{k-2}{3}} m_{1} P_{k}^{1}(x, y) + \sum_{k \geq 2} m_{3}^{\frac{k-2}{3}} m_{2} P_{k}^{2}(x, y).$$

The term

$$m_3^{-1/3}(x_3x + y_3y + P_1^1 + P_1^2) + \sum_{k>2} m_3^{\frac{k-2}{3}} m_1 P_k^1(x,y) + \sum_{k>2} m_3^{\frac{k-2}{3}} m_2 P_k^2(x,y)$$

was already computed for the circular case H_{CR4BP} , so if we use these computations we can write

$$H_1 = \frac{1}{2}(x^2 + y^2) + \frac{1}{\sqrt{x^2 + y^2}} + m_1 P_2^1 + m_2 P_2^2 + \mathcal{O}(m_3^{1/3}).$$

Finally, taking the limit $m_3 \to 0$ we obtain

$$H_1 = \frac{1}{2}(x^2 + y^2) + \frac{1}{\sqrt{x^2 + y^2}} - \frac{1}{8}x^2 + \frac{3\sqrt{3}}{4}(1 - 2\mu)xy + \frac{5}{8}y^2,$$

as desired.

We can rotate the coordinate system so that the axis from the center of mass to m_3 becomes the x-axis:

Corollary 3.2. The Hamiltonian (17) can be written, after a coordinate rotation which has eigenvalues $\lambda_1 = \frac{3}{2}(1-d)$ and $\lambda_2 = \frac{3}{2}(1+d)$, where $d=\sqrt{1-3\mu+3\mu^2}$, in the form

(22)
$$H_{CH4BP} = \frac{1}{2}(p_x^2 + p_y^2) + yp_x - xp_y - U_{rot}(x, y),$$

with

(23)
$$U_{rot} = -ax^2 - by^2 + \frac{1}{\sqrt{x^2 + y^2}}$$

where $a = \frac{1}{2}(1 - \lambda_2)$ and $b = \frac{1}{2}(1 - \lambda_1)$. The effective potential is

(24)
$$\Omega_{eff} = \frac{1}{2}(x^2 + y^2) + U_{rot}(x, y) = \frac{1}{2}(\lambda_2 x^2 + \lambda_1 y^2) + \frac{1}{\sqrt{x^2 + y^2}}$$

so

(25)
$$H_{CH4BP} = \frac{1}{2}(p_x + y)^2 + \frac{1}{2}(p_y - x)^2 - \Omega_{eff}(x, y).$$

The Hamiltonian (19) can be written as

(26)
$$H_{EH4BP} = H_{CH4BP} + \epsilon \cos(f) \left(\frac{1}{2} (x^2 + y^2) + U_{rot}(x, y) \right).$$

4. Equilibrium points, Hill regions, and invariant manifolds in тне СН4ВР

We assume $\mu = 0.00095$, representing the relative mass of Jupiter in the Sun-Jupiter system.

For the case when $\epsilon = 0$, we obtain the circular Hill Four-Body Problem (CH4BP) which is described by the Hamiltonian H_{CH4BP} given by (19). After applying a rotation of coordinates, as in Corollary 3.2, the Hamiltonian of the CH4BP reduces to:

(27)
$$H_{CH4BP} = \frac{1}{2}(p_x^2 + p_y^2) + yp_x - xp_y - U_{rot}(x, y).$$

The equations of motion possess the following symmetries:

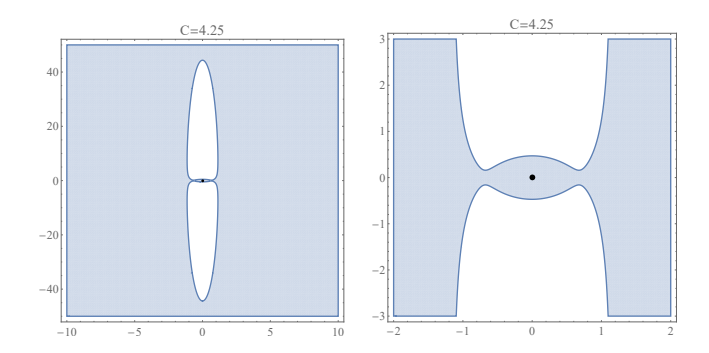


FIGURE 2. Hill's region for the CH4BP for $\mu = 0.00095$ and h = -2.125. The second figure is a magnification of the first one.

- $S(x,y,\dot{x},\dot{y},t)=(x,-y,-\dot{x},\dot{y},-t)$, with respect to the x-axis; $S'(x,y,\dot{x},\dot{y},t)=(-x,y,\dot{x},-\dot{y},-t)$, with respect to the y-axis; $S''=S\circ S'(x,y,\dot{x},\dot{y},t)=(-x,-y,-\dot{x},-\dot{y},t)$, the composition of Sand S', with respect to the origin.

The equations of motion for the circular case have 4 equilibrium points given by the coordinates

$$L_1 = \left(\frac{1}{\sqrt[3]{\lambda_2}}, 0\right), L_2 = \left(-\frac{1}{\sqrt[3]{\lambda_2}}, 0\right), L_3 = \left(0, \frac{1}{\sqrt[3]{\lambda_1}}\right), L_4 = \left(0, -\frac{1}{\sqrt[3]{\lambda_1}}\right).$$

The linear stability of L_1 and L_2 is of center-saddle type, for all μ , while that of L_3 and L_4 is of center-center type, for μ less or equal than some critical value μ_{cr} , and of complex-saddle type otherwise; see [BGG15]. The value of the energy H_{CH4BP} at the equilibrium point L_1 is $h_{L_1} = -2.16286$. In Fig. 2 we show the Hill regions

$$\{(x,y) \mid \Omega_{eff} \ge -h\}$$

for the value h = -2.125 of H_{CH4BP} , where we observe the inner region around the tertiary connected with the outer region through two 'bottlenecks', which become wider as we increase the energy level h.

We compute numerically the stable W^s and unstable W^u manifolds of the Lyapunov orbits for the saddle-center equilibrium points L_1 and L_2 , using the (x, y, \dot{x}, \dot{y}) coordinates, where $\dot{x} = p_x + y$ and $\dot{y} = p_y - x$. We also compute the intersection of these manifold with the section

$$\Sigma := \{ (x, y, \dot{x}, \dot{y}) \in \mathbb{R}^4 \mid y = 0 \}.$$

In the (x,y)-configuration space, y=0 corresponds to intersections with the x-axis.

We show the evolution of the invariant manifolds in the plane (x, \dot{x}) for some values of the energy level h in Fig. 3. It is notable that the invariant manifolds in the unbounded outer region do not escape to infinity, as in the lunar Hill's problem. In Fig. 4 we show the first intersections between the

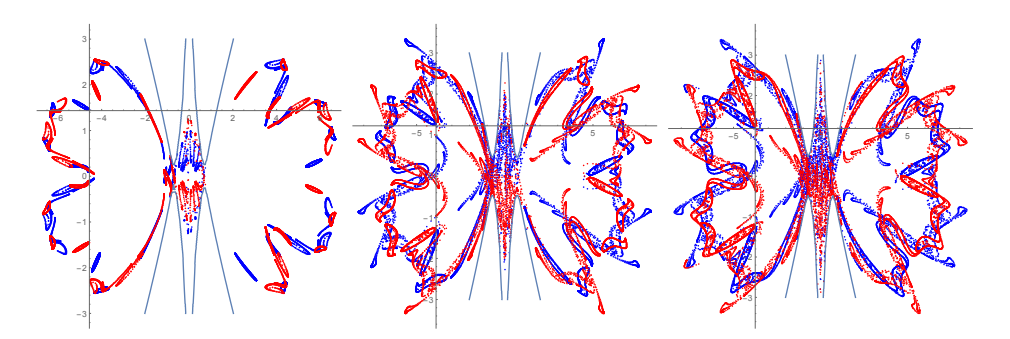


FIGURE 3. Stable (red) and unstable (blue) manifolds after 25 cuts with the Poincaré section Σ , and tangency curve (grey) in the plane (x, \dot{x}) , corresponding to trajectories that intersect Σ tangentially: h = -2.15 (left); h = -2.075 (center); h = -2.0 (right).

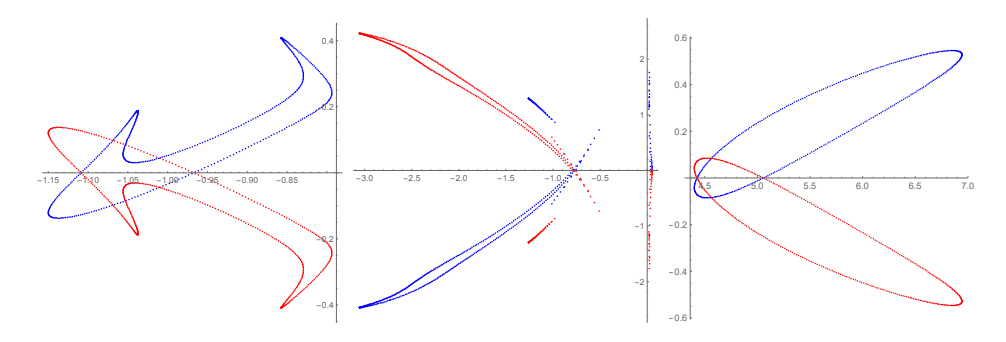


FIGURE 4. First intersections between the invariant manifolds for: inner region h = -2.15 (left); inner region h = -2.075 (center); outer region h = -2.0 (right).

invariant manifolds in the inner and outer region, where we note the presence of symmetric intersections ($\dot{x}=0$) which correspond to homoclinic orbits symmetric with respect to the x-axis. In Fig. 5 we show two symmetric homoclinic orbits in the outer region. The computations were performed using a linear approximation around the periodic orbits and integrating numerically the vector field with tolerances for the error of order of machine epsilon.

5. The mechanism of diffusion in the elliptic problem

In the previous section we showed that the elliptic problem for small values of the eccentricity can be written as

$$H_{EH4BP} = H_{CH4BP} + \epsilon \cos(f)H_1 + O(\epsilon^2),$$

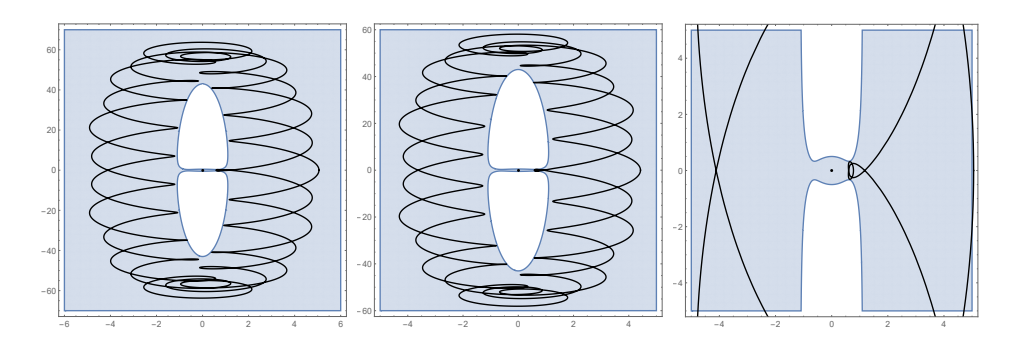


FIGURE 5. Homoclinic orbits corresponding to the points (5.05682901163445,0) and (4.42411675944339,0) in the (x,\dot{x}) -plane for h=-2.0. Magnification of the homoclinic orbit for $x_0=5.05682901163445$.

where H_{CH4BP} is the Hamiltonian of the circular Hill problem, f is the new time variable (which is 2π -periodic), ϵ is the eccentricity, and

$$H_1 = \frac{1}{2}(x^2 + y^2) + U_{rot}(x, y),$$

with $U_{rot}(x,y)$ given by (23). This is a time-dependent perturbation of H_{CH4BP} , with perturbation parameter ϵ . Let

$$G(x, y, t) := \cos(t)H_1(x, y),$$

so the Hamiltonian that we consider is

(28)
$$H_{\epsilon}(x, y, p_x, p_y, t) = H_0(x, y, p_x, p_y) + \epsilon G(x, y, t) + O(\epsilon^2),$$

Here we simplified the notation $H_{\epsilon} = H_{EH4BP}$, $H_0 = H_{CH4BP}$, and t = f. We now formulate the main theoretical result on Arnold diffusion:

Theorem 5.1. Consider the dynamics of the 2π -map f_{ϵ} associated to the flow system (28). Assume that the following conditions are satisfied for all energy levels h within some range $[h_{\alpha}, h_{\beta}]$ of H_0 :

- (i) The unperturbed system for $\epsilon = 0$ possesses two NHIM's Λ_0^i , consisting of periodic orbits $\lambda^i(h)$ around L_i , for i = 1, 2.
- (ii) The NHIM's for $\epsilon = 0$ can be parametrized in terms of symplectic action-angle coordinates (I_i, θ_i) , with the coordinate $I_1 = I_2$ uniquely determined by h.
- (iii) The corresponding stable and unstable manifolds $W^s(\Lambda_0^j)$, $W^u(\Lambda_0^i)$, intersects transversally for i, j = 1, 2.
- (iv) There exists a collection of scattering maps $\{\sigma_0^i\}$ associated to the transverse homoclinic connections $W^u(\Lambda_0^i) \cap W^s(\Lambda_0^i)$, i=1,2, as well as a collection of scattering maps $\{\sigma_0^{i,j}\}$ associated to the transverse heteroclinic connections $W^u(\Lambda_0^i) \cap W^s(\Lambda_0^j)$, $i \neq j$, such that,

each scattering map expressed in the appropriate action-angle coordinate is of the form

$$(I, \theta) \mapsto (I, \theta + \Delta(I))$$

where Δ depends on the scattering map and on h.

(v) Each perturbed scattering map associated to a transverse homoclinic / heteroclinic connections is of the form

(29)
$$\sigma_{\epsilon}(I,\theta) = (I,\theta + \Delta(I)) + \epsilon J \nabla S(I,\theta + \Delta(I)) + O(\epsilon^{2}),$$

for some function $S = S(I, \theta)$ depending on the scattering map.

(vi) Assume that the perturbed scattering maps satisfy satisfy the nondegeneracy conditions (50), (51), (52), (53), (54) from Proposition 5.7.

Then, there exist $\epsilon_0 > 0$ and energy levels $h_{\alpha} < h_{\beta}$, such that, for all $0 < \epsilon < \epsilon_0$, there exists a diffusing orbit $\Phi_{\epsilon}^t(z)$ of the perturbed system and $T = T(\epsilon) > 0$ such that

$$H_0(z) < \tilde{h}_{\alpha} \text{ and } H_0(\Phi_{\epsilon}^T(z)) > \tilde{h}_{\beta}.$$

Moreover, there exist diffusing orbits that closely follow the homoclinic connections, as well as diffusing orbits that follow the heteroclinic connections.

The NHIM's assumed in (i) will be described in Section 5.1. The actionangle coordinates assumed in (ii) will be introduced in Section 5.2. In Section 5.3, we will first recall the scattering map and the formula for Hamiltonian function that generates it, and then we provide formulas for the scattering map in the case of the EH4BP. In Section 5.4 we provide a general result – Proposition 5.7 – from which Theorem 5.1 immediately follows. The numerical verification of the conditions of Theorem 5.1 is done in Section 6.

- Remark 5.2. It is clear that the change of coordinates from the inertial non-rotating system to the pulsating system involves the perturbation parameter (similar changes of coordinates can be found in [Sze67, Bel04]). The main point is to obtain a system of the form (28) in such a way that H_0 possesses a normal hyperbolic invariant manifold and transverse intersections between its stable and unstable manifolds. The model considered here satisfies these requirements. The effect of the parameter ϵ in the geometry of the coordinates could be relevant only if we consider the original non-rotating inertial system, which is not the case in the current work.
- 5.1. The unperturbed NHIM's. We consider the unperturbed system corresponding to $\epsilon = 0$. For each center-saddle equilibrium point L_i , i = 1, 2, we consider a family of Lyapunov orbits $\lambda_i(h)$ associated to energy levels h within some suitable energy range $[h_{\alpha}, h_{\beta}]$ (to be specified later).

Due to the symmetry $S'(x, y, p_x, p_y) = (-x, y, p_x, -p_y)$, the Lyapunov orbits $\lambda_i(h)$, i = 1, 2, form a symmetric pair. The Lyapunov orbits about L_1 and L_2 are both traveled clockwise. The existence of Lyapunov orbits about

the points L_i , i = 1, 2, follows from the Lyapunov Center Theorem [Mos58], for energy levels near the critical energy $h_{L_1} = H_0(L_1) = H_0(L_2)$. These orbits can be computed by numerical continuation for higher energy levels, up to collision with m_3 . Their existence can be established rigorously via computer assisted proofs [Cap12]. In this paper we have non-rigorous computations of the Lyapunov orbits for the specific energy levels considered.

The family of Lyapunov orbits for the energy range $[h_{\alpha}, h_{\beta}]$ determines

(30)
$$\Lambda_0^i = \bigcup_{h \in [h_\alpha, h_\beta]} \lambda_i(h), \text{ for } i = 1, 2,$$

which is a 2-dimensional NHIM with boundary for the unperturbed flow Φ_0^t of H_0 .

5.2. Coordinate systems on the NHIM's and inner dynamics. Below we provide some parametrizations for the NHIM's. We focus on Λ_0^1 ; a similar parametrization can be obtained for Λ_0^2 .

Each Lyapunov periodic orbit $\lambda_1(h)$ intersects the x-axis in precisely two points, each of the form $(q,p)=(x,0,0,p_y)$, one on the left of L_1 and the other on the right of L_1 . Let $(x^*,0,0,p_y^*)$ be the intersection between the Lyapunov orbit and the x-axis on the left of L_1 , which is characterized by $p_y^*>0$. The orbit $\lambda_1(h)$ is uniquely determined by the coordinate $x^*=x^*(h)$, as the coordinate $p_y^*=p_y^*(h)$ follows implicitly from the energy condition. Let T(h) be the period of $\lambda_1(h)$. Since the energy level is uniquely determined by x^* , we can also write $T(h)=T(x^*)$ for $x^*=x^*(h)$. Then the Lyapunov periodic orbit is given by

$$\lambda_1(h) = \{ \Phi_0^t(x^*(h), 0, 0, p_u^*(h)) \mid t \in \mathbb{R}/(T(h)\mathbb{Z}) \}.$$

Then the NHIM Λ_0^1 can be described as

(31)
$$\Lambda_0^1 = \bigcup_{h \in [h_{\alpha}, h_{\beta}]} \lambda_1(h) \\
= \{\Phi_0^t(x^*(h), 0, 0, p_y^*(h)) \mid t \in \mathbb{R}/(T(h)\mathbb{Z}) \text{ for } h \in [h_{\alpha}, h_{\beta}]\},$$

and can be parametrized by (x^*, t^*) for $x^* \in [x^*(h_\alpha), x^*(h_\beta)]$ and $t^* \in \mathbb{R}/(T(h)\mathbb{Z})$, where $x^* = x^*(h)$ for $h \in [h_\alpha, h_\beta]$. The coordinate system (x^*, t^*) is not symplectic on Λ_0^1 .

We define symplectic coordinates (I,θ) on Λ_0^1 as follows. Let $\omega_{\Lambda_0^1} = (dp \wedge dq)_{\Lambda_0^1} := (dp_x \wedge dx + dp_y \wedge dy)_{\Lambda_0^1}$ be the induced symplectic form on Λ_0^1 ; since the induced form is non-degenerate, it endows Λ_0^1 with a symplectic structure [DdlLS08]. Let

$$\theta = \frac{t^*}{T(x^*)}$$
 and $I = \int_{\lambda_0^1(h)} p dq$.

The action I = I(h) is uniquely determined by the energy level h, and corresponds to a unique Lyapunov orbit. We then have

$$dI \wedge d\theta = \omega_{|\Lambda_0^1}.$$

The condition $h \in [h_{\alpha}, h_{\beta}]$ implies that $I \in [I_{\alpha}, I_{\beta}]$ for $I_{\alpha} = I(h_{\alpha}) = I(x^*(h_{\alpha}))$ and $I_{\beta} = I(h_{\beta}) = I(x^*(h_{\beta}))$. Each $I \in [I_{\alpha}, I_{\beta}]$ is in unique correspondence with some $h \in [h_{\alpha}, h_{\beta}]$ as well as with some $x^* \in [x^*(h_{\alpha}), x^*(h_{\beta})]$, so we can write $T(I) = T(x^*(I))$.

We define the reference manifold

$$N = \{(I, \theta) \mid I \in [I_{\alpha}, I_{\beta}], \ \theta \in \mathbb{T}^1\}$$

and the parametrization of Λ_0^1 given by

$$k_0: N \to \Lambda_0^1$$
, where $k_0(I, \theta) = \Phi_0^{\theta T(I)}(x^*(I), 0, 0, p_y^*(I))$.

The parametrization k_0 induces a flow \mathbb{R}^t on \mathbb{N} given by

$$R^{t}(I,\theta) = (I,\theta + \omega t)$$
 where $\omega = \frac{1}{T(I)}$.

We have the following conjugacy

$$N \xrightarrow{R^t} N$$

$$k_0 \downarrow \qquad \qquad \downarrow k_0$$

$$\Lambda_0^1 \xrightarrow{\Phi_0^t} \Lambda_0^1$$

When we consider both NHIM's Λ_0^1 , Λ_0^2 , we have the corresponding (x_1^*, t_1^*) and (x_2^*, t_2^*) -coordinates, and the action-angle coordinates (I_1, θ_1) and (I_2, θ_2) . By the symmetry of the Lyapunov orbits $x_2^* = -x_1^*$. The angle θ_1 is measured clockwise starting from the point $(x_1^*, 0, 0, p_{1,y}^*)$, and the angle θ_2 is measured clockwise starting from the point $(x_2^*, 0, 0, p_{2,y}^*)$. Since the action I is uniquely determined by the energy level $H_0 = h$, the action coordinate is the same $I_1 = I_2 := I$ for both NHIM's.

- 5.3. The scattering map. In Sections 5.1 we have identified two NHIM's, as well as homoclinic and heteroclinic connections between them. Moving along the homoclinic / heteroclinic orbits represents the outer dynamics. The outer dynamics can be described by scattering maps. First we review the definition of the scattering map and its properties, following [DdlLS08]. Second, we describe the scattering map for the unperturbed problem, that is, in the context of the CH4BP.
- 5.3.1. The scattering map: definition and properties. Consider the general case of a normally hyperbolic invariant manifold Λ for a flow Φ^t on some smooth manifold M. We assume that M and Φ^t are sufficiently regular; explicit regularity conditions can be found in [DdlLS08]. Let $W^s(\Lambda)$, $W^u(\Lambda)$

be the stable and unstable manifolds of Λ . Define the wave maps as canonical projections along fibers, i.e.,

$$\Omega^+: W^s(\Lambda) \to \Lambda,$$

 $\Omega^-: W^u(\Lambda) \to \Lambda,$

where Ω^+ assigns to $z \in W^s(\Lambda)$ its stable foot point $z^+ = \Omega^+(z)$, uniquely defined by $z \in W^s(z^+)$, and, similarly, Ω^- assigns to $z \in W^u(\Lambda)$ its unstable footpoint $z^- = \Omega^-(z)$, uniquely defined by $z \in W^u(z^-)$.

The wave maps satisfy the following equivariance property

$$\Omega^{\pm} \circ \Phi^t = \Phi^t \circ \Omega^{\pm}.$$

A homoclinic channel Γ is a submanifold in $W^u(\Lambda) \cap W^s(\Lambda)$ that satisfies the following strong transversality conditions for all $z \in \Gamma$:

(33)
$$T_z\Gamma = T_zW^s(\Lambda) \cap T_zW^u(\Lambda),$$
$$T_zM = T_z\Gamma \oplus T_zW^u(z^-) \oplus T_xW^s(z^+),$$

and such that

$$\Omega_{\Gamma}^{\pm}:\Gamma\to\Omega^{\pm}(\Gamma)$$
 is a diffeomorphism.

Then, the scattering map associated to the homoclinic channel Γ is the mapping

(34)
$$\sigma = \sigma^{\Gamma} : \Omega^{-}(\Gamma) \subseteq \Lambda \to \Omega^{+}(\Gamma) \subseteq \Lambda, \\ \sigma = \Omega_{|\Gamma}^{+} \circ (\Omega_{|\Gamma}^{-})^{-1}.$$

The map σ is a diffeomorphism from its domain onto its image in Λ . We have that $\sigma(z^-) = z^+$ if and only if

(35)
$$d(\Phi^{-T_{-}}(z), \Phi^{-T_{-}}(z^{-})) \to 0$$
, and $d(\Phi^{T_{+}}(z), \Phi^{T_{+}}(z^{+})) \to 0$

as $T_-, T_+ \to +\infty$, respectively, for some uniquely defined $z \in \Gamma$.

The equivariance of the wave maps yields the following equivariance property of the scattering map:

(36)
$$\Phi^t \circ \sigma^{\Gamma} = \sigma^{\Phi^t(\Gamma)} \circ \Phi^t.$$

An important property of the scattering map is that σ is symplectic provided that M, Λ, Φ^t are symplectic.

Remark 5.3. If the strong transversality condition (33) is satisfied at a point z_* , then it is satisfied in a small neighborhood Γ_* of z_* in $W^u(\Lambda) \cap W^s(\Lambda)$. One can take Γ_* as a homoclinic channel and define the associated scattering map, and then extend Γ_* to a maximal domain on which the wave maps $\Omega_{|\Gamma_*}^{\pm}$ are diffeomorphisms. Extending Γ_* beyond its maximal domain may result in failure of monodromy. Monodromy here means that when the scattering map is applied to (I, θ) and to $(I, \theta + 1)$ it gives the same value, in other words the scattering map is well defined as a map on the annulus, since θ is defined mod 1; this does not happen in general, see [CGDIL17].

For example, consider the homoclinic orbit $\Phi^t(z_*)$; each point z on this homoclinic orbit is of the form $z = \Phi^t(z_*)$ for some t. The equivariance property (32) implies

(37)
$$\Omega^{\pm}(z) = \Omega^{\pm}(\Phi^{t}(z_{*})) = \Phi^{t} \circ \Omega^{\pm}(z_{*}) = \Phi^{t}(z_{*}^{\pm}).$$

Therefore, it is possible to have a pair of points $z_1 = \Phi^{t_1}(z_*)$, $z_2 = \Phi^{t_2}(z_*)$ such that $\Omega^-(z_1) = \Omega^-(z_2)$ and $\Omega^+(z_1) \neq \Omega^+(z_2)$, so $\Omega^+ \circ (\Omega^-)^{-1}$ is not a well-defined map. Restricting to a suitable Γ^* will ensure the monodromy property.

An alternative is to define a scattering correspondence rather than a scattering map, which allows for assigning to a given point z^- multiple points z^+ ; see [GM22].

We now consider the scattering map in the case of a perturbed system. Consider a family of NHIM's Λ_{ϵ} for Φ_{ϵ}^{t} on M, for $0 \leq \epsilon < \epsilon_{0}$. We will implicitly assume that Φ_{ϵ}^{t} and Λ_{ϵ} are sufficiently regular in the variables and in the parameter ϵ . Here we view Φ_{ϵ}^{t} as a perturbation of Φ_{0}^{t} . Below, we will also consider the special case when the flow Φ_{ϵ}^{t} is the flow of a perturbed Hamiltonian system H_{ϵ} .

Assume that Λ_{ϵ} has a smooth parametrization in terms of some reference manifold N, that is, there exists a family of diffeomorphisms (in a suitable regularity class)

$$k_{\epsilon}: N \to \Lambda_{\epsilon} = k_{\epsilon}(N), \text{ for } 0 \le \epsilon < \epsilon_0.$$

Assume that $W^u(\Lambda_{\epsilon})$ and $W^s(\Lambda_{\epsilon})$ intersect transversally along a homoclinic channel Γ_{ϵ} . Let $\sigma_{\epsilon}: \Omega^-(\Gamma_{\epsilon}) \subseteq \Lambda_{\epsilon} \to \Omega^+(\Gamma_{\epsilon}) \subseteq \Lambda_{\epsilon}$ be the scattering map associated to Γ_{ϵ} .

This is induces a locally defined diffeomorphism on N given by

$$s_{\epsilon} = k_{\epsilon}^{-1} \circ \sigma_{\epsilon} \circ k_{\epsilon}.$$

We will also refer to s_{ϵ} as the scattering map. Note that for all ϵ the map s_{ϵ} is a diffeomorphism on some subset of the same manifold N, in contrast with σ_{ϵ} , which is a diffeomorphism on some subset of a manifold Λ_{ϵ} that depends on ϵ . The advantage of using the scattering map s_{ϵ} induced on the reference manifold N is that one can compare s_{ϵ} 's for different parameter values ϵ .

It turns out that the perturbed scattering map s_{ϵ} can be expanded in powers of ϵ as follows

(38)
$$s_{\epsilon}(I,\theta) = s_{0}(I,\theta) + \epsilon J \nabla S \circ s_{0}(I,\theta) + O(\epsilon^{2})$$
$$= s_{0}(I,\theta) + \epsilon \left(-\frac{\partial S}{\partial \theta}, \frac{\partial S}{\partial I}\right) \circ s_{0}(I,\theta) + O(\epsilon^{2})$$

for some Hamiltonian function S defined on some domain in N. Above, s_0 is the scattering map induced by σ_0 , corresponding to the unperturbed system.

In the perturbative setting S can be computed explicitly. In the context of a perturbed Hamiltonian system H_{ϵ} , S can be computed as a Melnikov integral

(39)
$$S(k_0^{-1}(z_0^+)) = \int_{-\infty}^0 \left[\frac{\partial H_{\epsilon}}{\partial \epsilon} \circ \Phi_0^t(z_0) - \frac{\partial H_{\epsilon}}{\partial \epsilon} |_{\epsilon=0} \circ \Phi_0^t(z_0^-) \right] dt + \int_0^{+\infty} \left[\frac{\partial H_{\epsilon}}{\partial \epsilon} |_{\epsilon=0} \circ \Phi_0^t(z_0) - \frac{\partial H_{\epsilon}}{\partial \epsilon} |_{\epsilon=0} \circ \Phi_0^t(z_0^+) \right] dt.$$

The integrals in (39) are improper integrals whose integrand is given by the difference between the perturbation evaluated on homoclinic orbits of the unperturbed system and the perturbation evaluated on the asymptotic orbits on the unperturbed NHIM. The improper integrals converge exponentially fast, so they can be efficiently computed via numerical methods.

In the context of Section 5.2, if $k_0^{-1}(z_0^+) = (I, \theta)$, then we can write S in terms of (I, θ) as

$$S(I,\theta) = \int_{-\infty}^{0} \left[\frac{\partial H_{\epsilon}}{\partial \epsilon} \circ \Phi_{0}^{t} \circ (\Omega^{-})^{-1} \circ \sigma_{0}^{-1} \circ k_{0}(I,\theta) \right] dt$$

$$-\frac{\partial H_{\epsilon}}{\partial \epsilon} |_{\epsilon=0} \circ \Phi_{0}^{t} \circ \sigma_{0}^{-1} \circ k_{0}(I,\theta) dt$$

$$+ \int_{0}^{+\infty} \left[\frac{\partial H_{\epsilon}}{\partial \epsilon} |_{\epsilon=0} \circ \Phi_{0}^{t} \circ (\Omega^{+})^{-1} \circ k_{0}(I,\theta) \right] dt$$

$$-\frac{\partial H_{\epsilon}}{\partial \epsilon} |_{\epsilon=0} \circ \Phi_{0}^{t} \circ k_{0}(I,\theta) dt,$$

It is clear that (40) is equivalent to (39) since, for $k_0^{-1}(z_0^+) = (I, \theta)$, we have

$$k_0(I,\theta) = z_0^+,$$

 $\sigma_0^{-1} \circ k_0(I,\theta) = z_0^-,$
 $(\Omega^-)^{-1} \circ \sigma_0^{-1} \circ k_0(I,\theta) = (\Omega^+)^{-1} \circ k_0(I,\theta) = z_0.$

The scattering map can be defined in a similar way for heteroclinic connections between two NHIM's Λ^1 and Λ^2 . Assuming that $W^u(\Lambda^2)$ intersects transversally $W^s(\Lambda^1)$, we can define wave maps

$$\Omega^{1,+}: W^s(\Lambda_1) \to \Lambda_1,$$

 $\Omega^{2,-}: W^u(\Lambda_2) \to \Lambda_2,$

and a heteroclinic channel $\Gamma \subseteq W^u(\Lambda^2) \cap W^s(\Lambda^1)$ in a similar fashion to the homoclinic case. Then we define

$$\sigma = \Omega_{|\Gamma}^{1,+} \circ (\Omega_{|\Gamma}^{2,-})^{-1}.$$

The scattering map in the heteroclinic case enjoys similar properties to the one for the scattering map in the homoclinic case.

In the sequel, we will use a two-dynamics approach: the outer dynamics, along homoclinic/heteroclinic orbits to the NHIM's, encoded by the scattering map, and the inner dynamics, defined as the restriction of the flow to the NHIM's. Note that both dynamics are defined on the NHIM's.

5.3.2. The unperturbed scattering map associated to homoclinic connections for the CH4BP. First, we show that, in general, the unperturbed scattering map associated to a homoclinic channel is a phase shift in the angle variable.

For a given range of energies $h \in [h_{\alpha}, h_{\beta}]$, let z = z(h) be a homoclinic point, z^{\pm} be its stable and unstable foot points, θ^{\pm} their corresponding angle coordinates, and T = T(h) the period of the Lyapunov orbit $\lambda(h)$. We can define the homoclinic channel

$$\Gamma = \bigcup_{\substack{h \in [h_{\alpha}, h_{\beta}] \\ \theta \in [\theta^{-}, 1 + \theta^{-}]}} \Phi_{0}^{(\theta - \theta^{-})T}(z).$$

The flow Φ_0^t acts on the fiber $W^u(z^-) = W^u(k_0(I,\theta^-))$ by shifting its base point $k_0(I,\theta^-)$ to $k_0(R^t(I,\theta^-)) = k_0(I,\theta^- + \frac{t}{T(I)})$, and on the fiber $W^s(z^+) = W^u(k_0(I,\theta^+))$ by shifting its base point $k_0(I,\theta^+)$ to $k_0(R^t(I,\theta^+)) = k_0(I,\theta^+ + \frac{t}{T(I)})$. The flow Φ_0^t takes $z \in W^u(z^-) \cap W^s(z^+)$ to $\Phi_0^t(z) \in W^u(\Phi_0^t(z^-)) \cap W^s(\Phi_0^t(z^+))$. In particular, for $t = (\theta - \theta^-)T$, we have

$$\Phi_0^{(\theta-\theta^-)T}(W^u(z^-)) = W^u(k_0(I,\theta)),$$

$$\Phi_0^{(\theta-\theta^-)T}(W^s(z^+)) = W^s(k_0(I,\theta+\theta^+-\theta^-)).$$

By the S-symmetry of the flow on the Lyapunov orbit we also have

$$\begin{split} \Phi_0^{(1+\theta-\theta^-)T}(W^u(z^-)) = & \Phi_0^{(\theta-\theta^-)T} \circ \Phi_0^T(W^u(z^-)) = \Phi_0^{(\theta-\theta^-)T}(W^u(\Phi_0^T(z^-)) \\ = & \Phi_0^{(\theta-\theta^-)T}(W^u(z^-)). \end{split}$$

and similarly

$$\Phi_0^{(1+\theta-\theta^+)T}(W^s(z^+)) = \Phi_0^{(\theta-\theta^+)T}(W^s(z^+)).$$

The following result [GdlLM22] gives a complete description of the unperturbed scattering map.

Lemma 5.4. The unperturbed scattering map is globally defined, and is given in the action-angle (I, θ) -coordinates by

$$\sigma_0(I, \theta^-) = (I, \theta^+) = (I, \theta^- + \Delta),$$

where I = I(h) and $\Delta = \Delta(h)$ depend on the energy level h.

Proof. Let $z_0 \in \Gamma$ be a homoclinic point. If $H_0(z) = h$. If $z_0^{\pm} = \Omega_{\pm}^{\Gamma}(z)$, then z_0^{\pm} are points on the Lyapunov orbit $\lambda(h)$. Let (I, θ_0^{\pm}) be the action-angle coordinates of z^{\pm} . Then $\sigma(z_0^-) = z_0^+$ is given in local coordinates by

$$s_0(I,\theta_0^-) = (I,\theta_0^+) := (I,\theta_0^- + \Delta).$$

where we denote $\Delta = \Delta(h) = \theta_0^+ - \theta_0^-$.

Then, if $z_1 \in \Gamma \cap \{H_0(z) = h\}$ is another homoclinic point, then $z_1 = \Phi_0^{t_1}(z_0)$ for some t_1 . Let (I, θ_1^{\pm}) be the action-angle coordinates of z_1^{\pm} , respectively. By the equivariance property (32), $z_1^{\pm} = \Omega_{\pm}^{\Gamma}(z_1) = \Omega_{\pm}^{\Gamma}(\Phi_0^{t_1}(z_0)) = \Phi_0^{t_1}(\Omega_{\pm}^{\Gamma}(z_0)) = \Phi_0^{t_1}(z_0^{\pm})$, therefore $\theta_1^{\pm} = \theta_0^{\pm} + \frac{1}{T}t_1$ so $\theta_1^{+} - \theta_1^{-} = \theta_0^{+} - \theta_0^{-}$, thus

$$s_0(I, \theta_1^-) = (I, \theta_1^- + \Delta).$$

5.3.3. The unperturbed NHIM's and scattering map in the extended phase space. Since the perturbation $G(t) = \epsilon \cos(t)H_1 + O(\epsilon^2)$ is time-periodic, it is convenient to consider time as an additional variable which we denote by s. The extended phase space is $M \times \mathbb{T}^1$. The equations of motion in the extended phase space are augmented with an equation for the evolution of the new variable $\frac{ds}{dt} = 1$. Denoting by $\tilde{\Phi}_0^t$ the flow in the extended space, we have $\tilde{\Phi}_0^t(z,s) = (\Phi_0^t(z),s+t)$.

In the extended space, the NHIM Λ_0^i corresponds to the NHIM

$$\tilde{\Lambda}_0^i = \Lambda_0^i \times \mathbb{T}^1.$$

Similarly, any homoclinic/heteroclinic channel Γ gives rise to a homoclinic/heteroclinic channel in the extended space

$$\tilde{\Gamma}_0 = \Gamma_0 \times \mathbb{T}^1$$
.

The scattering map corresponding to σ_0 in the extended space is given by

$$\tilde{\sigma}_0(z,s) = (\sigma_0(z),s)$$

5.3.4. The perturbed NHIM's. We now consider the effect of the perturbation $G(t) = \epsilon \cos(s) H_1 + O(\epsilon^2)$ on the NHIM's in the extended phase space. We denote by $\tilde{\Phi}_{\epsilon}^t$ the extended flow.

The standard theory of normally hyperbolic invariant manifolds, [Fen72, HPS77] shows the persistence of compact NHIM's (without boundary) under small perturbations. In the case of manifolds with boundary, the theory only guarantees the persistence of a normally hyperbolic manifold that is locally invariant but not necessarily unique (see [BLZ00, BB13, E+13]). The proof in that case involves extending the vector field in such a way that the manifold we consider is an invariant manifold without boundary. Then, applying the result of persistence of an invariant manifold without boundary, one obtains the existence of a locally invariant manifold. The persistent manifold depends on the extension considered, and hence is not unique. However, all orbits that remain in a small neighborhood of the manifold and away from its boundary remain present in all extensions that do not modify the dynamics in that neighborhood.

This theory implies that there exists ϵ_0 such that the NHIM Λ_0^i , i=1,2, persists as a normally hyperbolic manifold $\tilde{\Lambda}_{\epsilon}^i$, which is locally invariant under the flow $\tilde{\Phi}_{\epsilon}^t$, for all $0 < \epsilon < \epsilon_0$. Moreover, there exists smooth parametrizations of these manifolds (see [DdlLS08]):

$$\tilde{k}_{\epsilon}: N \times \mathbb{T}^1 \to \tilde{\Lambda}_{\epsilon}.$$

Choosing ϵ_0 sufficiently small ensures that the transverse homoclinic/heteroclinic channels for the unperturbed system also persist as homoclinic/heteroclinic channels $\tilde{\Gamma}_{\epsilon}$ for $\tilde{\Phi}_{\epsilon}^{t}$. Therefore, we have a scattering map $\tilde{\sigma}_{\epsilon}$ associated to each channel. To compute the perturbed scattering map, we use (38). Since we work in the extended space the formula (40) for S becomes

$$S(I,\theta,s) = \int_{-\infty}^{0} \left[\left(\frac{\partial H_{\epsilon}}{\partial \epsilon} \circ \Phi_{0}^{t} \circ (\Omega^{-})^{-1} \circ \sigma_{0}^{-1} \circ k_{0}(I,\theta), s + t \right) - \left(\frac{\partial H_{\epsilon}}{\partial \epsilon} |_{\epsilon=0} \circ \Phi_{0}^{t} \circ \sigma_{0}^{-1} \circ k_{0}(I,\theta), s + t \right) \right] dt$$

$$+ \int_{0}^{+\infty} \left[\left(\frac{\partial H_{\epsilon}}{\partial \epsilon} |_{\epsilon=0} \circ \Phi_{0}^{t} \circ (\Omega^{+})^{-1} \circ k_{0}(I,\theta), s + t \right) - \left(\frac{\partial H_{\epsilon}}{\partial \epsilon} |_{\epsilon=0} \circ \Phi_{0}^{t} \circ k_{0}(I,\theta), s + t \right) \right] dt.$$

$$(41)$$

In the subsequent sections, we will compute the perturbed scattering map for the EH4BP.

5.3.5. The perturbed scattering map in the EH4BP. Consider a homoclinic channel $\tilde{\Gamma}_{\epsilon}$. The unperturbed scattering map (68) in (I, θ) -coordinate is given by

$$\tilde{\sigma}_0(I, \theta, t) = (I, \theta + \Delta, t)$$
 where $\Delta = \Delta(h)$.

Then we have

(42)
$$k_0^{-1}(\Omega_0^-(\Phi^{(\theta-\theta^-)T(I)}(z))) = (I,\theta),$$
$$k_0^{-1}(\Omega_0^+(\Phi^{(\theta-\theta^-)T(I)}(z))) = (I,\theta+\Delta),$$
$$s_0(I,\theta) = (I,\theta+\Delta).$$

To compute the perturbed scattering map $\tilde{\sigma}_{\epsilon}$ we use (38) where S is given by (41).

We recall that

$$\frac{\partial H_{\epsilon}}{\partial \epsilon}_{|\epsilon=0}(z,s) = G(z,s) = \cos(s)H_{1}(z)$$

$$(\Omega_{0}^{-})^{-1}(k_{0}(s_{0}^{-1}(I,\theta))) = (\Omega_{0}^{-})^{-1}(k_{0}(I,\theta-\Delta)) = \Phi^{(\theta+\theta^{-})T(I)}(z),$$

$$s_{0}^{-1}(I,\theta) = (I,\theta-\Delta) = (I,\theta+2\theta^{-}),$$

$$(\Omega_{0}^{+})^{-1}(k_{0}(I,\theta)) = \Phi_{0}^{(\theta+\theta^{-})T(I)}(z).$$

Substituting in (40) we obtain

(43)
$$S(I,\theta,s) = \int_{-\infty}^{0} \left[G(\Phi_0^{t+(\theta+\theta^-)T(I)}(z), t+s) \right] dt + \int_{0}^{+\infty} \left[G(\Phi_0^{t+(\theta+\theta^-)T(I)}(z), t+s) \right] dt - G(\Phi_0^{t}(I,\theta), t+s) \right] dt.$$

For our particular case of the EH4BP we have the following:

Proposition 5.5. In the EH4BP, the derivative with respect to the angle variable of the Hamiltonian that generates the scattering map in the extended phase space is given by the expression

$$(44) \frac{d}{d\theta}S(s_{0}(I,\theta),s) = T(I)\cos(s) \left[H_{1}(\Phi_{0}^{(\theta-\theta^{-})T(I)}(k_{0}(I,\theta^{+}))) - H_{1}(\Phi_{0}^{(\theta-\theta^{-})T(I)}(k_{0}(I,\theta^{-}))) \right]$$

$$+ T(I) \int_{-\infty}^{0} \sin(t+s) \left[H_{1}(\Phi_{0}^{t+(\theta-\theta^{-})T(I)}(z)) - H_{1}(\Phi_{0}^{t+(\theta-\theta^{-})T(I)}(k_{0}(I,\theta^{-}))) \right] dt$$

$$+ T(I) \int_{0}^{+\infty} \sin(t+s) \left[H_{1}(\Phi_{0}^{t+(\theta-\theta^{-})T(I)}(z)) - H_{1}(\Phi_{0}^{t+(\theta-\theta^{-})T(I)}(k_{0}(I,\theta^{+}))) \right] dt$$

Proof. We will use the fact that the perturbation is a separable function, i.e., $G(z,s) = \cos(s)H_1(z)$. We will also use that

$$\Phi^t(k_0(I,\theta)) = k_0(R^t(I,\theta)) = k_0(I,\theta + t\omega(I)).$$

We perform the change of variable $\tau = t + (\theta + \theta^{-})T(I)$ in (43). We note that, under this change of variable, we have

$$\begin{split} \Phi_0^t(k_0(I,\theta+2\theta^-)) = & \Phi_0^{\tau-(\theta+\theta^-)T(I)}(k_0(I,\theta+2\theta^-)) \\ = & \Phi_0^\tau(k_0(I,\theta+2\theta^- - (\theta+\theta^-)T(I)\omega(I))) \\ = & \Phi_0^\tau(k_0(I,\theta^-)) \end{split}$$

since $T(I)\omega(I) = 1$. Similarly,

$$\begin{aligned} \Phi_0^t(k_0(I,\theta)) = & \Phi_0^\tau(k_0(I,\theta - (\theta + \theta^-)T(I)\omega(I))) \\ = & \Phi_0^\tau(k_0(I,-\theta^-)) = \Phi_0^\tau(k_0(I,\theta^+)). \end{aligned}$$

The last equality is by the S-symmetry.

We obtain

$$S(I, \theta, s) = \int_{-\infty}^{(\theta + \theta^{-})T(I)} \cos(s + \tau - (\theta + \theta^{-})T(I)) \left[H_{1}(\Phi_{0}^{\tau}(z)) - H_{1}(\Phi_{0}^{\tau}(k_{0}(I, \theta^{-}))) \right] d\tau$$

$$+ \int_{(\theta + \theta^{-})T(I)}^{+\infty} \cos(s + \tau - (\theta + \theta^{-})T(I)) \left[H_{1}(\Phi_{0}^{\tau}(z)) - H_{1}(\Phi_{0}^{\tau}(k_{0}(I, \theta^{+}))) \right] d\tau.$$

We recall the following property

(46)
$$\frac{d}{d\theta} \int_{a(\theta)}^{b(\theta)} f(x,\theta) dx = \int_{a(\theta)}^{b(\theta)} \frac{\partial}{\partial \theta} f(x,\theta) dx + f(b(\theta),\theta)b'(\theta) - f(a(\theta),\theta)a'(\theta).$$

We apply (46) to (45), first, for $a(\theta) = -\infty$ and $b(\theta) = (\theta + \theta^-)T(I)$, and second for $a(\theta) = (\theta + \theta^-)T(I)$ and $b(\theta) = +\infty$. Since the integrands in (45) converge to 0 exponentially fast as $t \to \pm \infty$, the terms corresponding to the infinite limits on the right hand side of (46) vanish. We obtain:

$$\frac{d}{d\theta}S(I,\theta,s) = T(I)\cos(s) \left[H_1(\Phi_0^{(\theta+\theta^-)T(I)}(z)) - H_1(\Phi_0^{(\theta+\theta^-)T(I)}(k_0(I,\theta^-))) \right]
- T(I)\cos(s) \left[H_1(\Phi_0^{(\theta+\theta^-)T(I)}(z)) - H_1(\Phi_0^{(\theta+\theta^-)T(I)}(k_0(I,\theta^+))) \right]
+ T(I) \int_{-\infty}^{(\theta+\theta^-)T(I)} \sin(s+\tau-(\theta+\theta^-)T(I)) \left[H_1(\Phi_0^{\tau}(z)) - H_1(\Phi_0^{\tau}(k_0(I,\theta^-))) \right] d\tau
+ T(I) \int_{(\theta+\theta^-)T(I)}^{+\infty} \sin(s+\tau-(\theta+\theta^-)T(I)) \left[H_1(\Phi_0^{\tau}(z)) - H_1(\Phi_0^{\tau}(k_0(I,\theta^+))) \right] d\tau.$$

After cancelations and changing the variable back $t = \tau - (\theta + \theta^{-})T(I)$ we obtain

$$\frac{d}{d\theta}S(I,\theta,s) = T(I)\cos(s) \left[H_1(\Phi_0^{(\theta+\theta^-)T(I)}(k_0(I,\theta^+))) - H_1(\Phi_0^{(\theta+\theta^-)T(I)}(k_0(I,\theta^-))) \right]
+ T(I) \int_{-\infty}^{0} \sin(s+t) \left[H_1(\Phi_0^{t+(\theta+\theta^-)T(I)}(z)) - H_1(\Phi_0^{t+(\theta+\theta^-)T(I)}(k_0(I,\theta^-))) \right] dt
+ T(I) \int_{0}^{+\infty} \sin(s+t) \left[H_1(\Phi_0^{t+(\theta+\theta^-)T(I)}(z)) - H_1(\Phi_0^{t+(\theta+\theta^-)T(I)}(k_0(I,\theta^+))) \right] dt.$$

Last, we calculate $\frac{d}{d\theta}S(s_0(I,\theta),\tau) = \frac{d}{d\theta}S(I,\theta-2\theta^-,\tau)$, obtaining

$$\frac{d}{d\theta}S(s_{0}(I,\theta),s) = T(I)\cos(s) \left[H_{1}(\Phi_{0}^{(\theta-\theta^{-})T(I)}(k_{0}(I,\theta^{+}))) - H_{1}(\Phi_{0}^{(\theta-\theta^{-})T(I)}(k_{0}(I,\theta^{-}))) \right]
+ T(I) \int_{-\infty}^{0} \sin(s+t) \left[H_{1}(\Phi_{0}^{t+(\theta-\theta^{-})T(I)}(z)) - H_{1}(\Phi_{0}^{t+(\theta-\theta^{-})T(I)}(k_{0}(I,\theta^{-}))) \right] dt
+ T(I) \int_{0}^{+\infty} \sin(s+t) \left[H_{1}(\Phi_{0}^{t+(\theta-\theta^{-})T(I)}(z)) - H_{1}(\Phi_{0}^{t+(\theta-\theta^{-})T(I)}(k_{0}(I,\theta^{+}))) \right] dt.$$

Remark 5.6. We can obtain in a similar fashion a formula for $\frac{\partial S}{\partial I}$; see [GdlLM22]. However, we do not need it in this paper.

5.3.6. Reduction to a Poincaré section. We switch from continuous-time (flow) dynamics to discrete-time dynamics by taking the time- 2π map of the extended flow. For some fixed s^* define

$$\Sigma_{s^*} = \{ (z, s) \, | \, s = s^* \}.$$

We denote by f_{ϵ} the time- 2π map of the extended flow. Then

$$\Lambda_{\epsilon} := \tilde{\Lambda}_{\epsilon} \cap \Sigma_{s^*}$$

is a NHIM for f_{ϵ} . Any scattering map for the extended flow $\tilde{\sigma}_{\epsilon}^{\tilde{\Gamma}_{\epsilon}}$ induces a scattering map on Λ_{ϵ} given by

$$\sigma_{\epsilon}^{\Gamma_{\epsilon}}(z) = \tilde{\sigma}_{\epsilon}^{\tilde{\Gamma}_{\epsilon}}(z, s^*) \text{ for } z \in \Omega^{-}(\tilde{\Gamma}_{\epsilon}) \cap \Lambda_{\epsilon},$$

where $\Gamma_{\epsilon} = \tilde{\Gamma}_{\epsilon} \cap \Sigma_{s^*}$.

5.4. Mechanism of diffusion based on several scattering maps. We describe a general mechanism of diffusion based on several scattering maps. To avoid notation overload, we will identify Λ_{ϵ} with $\mathbb{T}^1 \times [I_{\alpha}, I_{\beta}]$ and the scattering map σ_{ϵ} on Λ_{ϵ} with its action-angle coordinate representation s_{ϵ} on $\mathbb{T}^1 \times [I_{\alpha}, I_{\beta}]$.

Assume that there exists a family of scattering maps $\sigma_{\epsilon}^{i}: \Omega^{-}(\Gamma^{i}) \to \Omega^{+}(\Gamma^{i}), i = 1, \ldots, L$, such that

(50)
$$\bigcup_{i=1,\dots,L} \Omega^{-}(\Gamma^{i}) \supseteq \mathbb{A},$$

where each scattering map σ^i_ϵ expressed in the action-angle coordinates is of the form

$$(51) \qquad \sigma^i_{\epsilon}(I,\theta) = (I,\theta + \Delta^i(I)) + \epsilon \left(-\frac{\partial S^i}{\partial \theta}, \frac{\partial S^i}{\partial I} \right) (I,\theta + \Delta^i(I)) + O(\epsilon^2),$$

for $(I, \theta) \in \Omega^{-}(\Gamma^{i}) \cap \mathbb{A}$.

Assume that A can be partition into finitely many strips S_i of the form

(52)
$$\mathcal{S}_i = \{ (I, \theta) \in \mathbb{A} \mid I \in [I_\alpha, I_\beta], \, \mathcal{C}^i(I) < \theta < \mathcal{C}^{i+1}(I) \},$$

where each $C^{i}(I)$ is a C^{1} -function in I, $C^{L+1} = C^{1}$, and

(53)
$$-\frac{\partial S^{i}}{\partial \theta}(I, \theta + \Delta^{i}(I)) \neq 0 \text{ for all } (I, \theta) \in \mathcal{S}_{i},$$

for i = 1, ..., L.

As such, each strip S_i is bounded by two C^1 -curves that run from the lower boundary of the annulus to the upper boundary. Any two strips S_i , S_j , $i \neq j$, are either disjoint or they only intersect along a boundary curve. On each strip S_i , the function $-\frac{\partial S^i}{\partial \theta}(I, \theta + \Delta^i(I))$ is either negative or positive. See Fig. 6

Assume that the following non-degeneracy condition holds

(54)
$$\sum_{i=1}^{L} \int_{\mathcal{S}_{i}} \left[-\frac{\partial S^{i}}{\partial \theta} (I, \theta + \Delta^{i}(I)) \right] dI \wedge d\theta \neq 0.$$

Proposition 5.7. Assume the conditions (50), (51), (52), (53), (54).

Then there exists $\epsilon_0 > 0$ and C > 0, such that for each $0 < \epsilon < \epsilon_0$ there exists an orbit (I_n, θ_n) , $n = 0, \ldots, N$, of the iterated function system generated by $\{\sigma_{\epsilon}^i\}_{i=1,\ldots,L}$ such that

$$|I_N - I_0| > C > 0.$$

Proof. Suppose that the sum of the integrals in (54) is positive. (A similar argument can be done when the sum is negative.) Then there exists $C_1 > 0$ such that:

(55)
$$\sum_{i=1}^{L} \int_{\mathcal{S}_i} \left[-\frac{\partial S^i}{\partial \theta} (I, \theta + \Delta^i(I)) \right] dI \wedge d\theta > C_1 > 0.$$

Define $\mathbb{A}' = \mathbb{T}^1 \times [I'_{\alpha}, I'_{\beta}]$ for some $I'_{\alpha} \gtrsim I_{\alpha}$ and $I'_{\beta} \lesssim I_{\beta}$. That is, the annulus A' is inside and slightly smaller than then annulus A. We will later impose additional conditions on I'_{α} and I'_{β} . Define the integrals

(56)
$$\mathcal{I}_{i} = \begin{cases} \int_{\mathcal{S}_{i} \cap \mathbb{A}'} \left[-\frac{\partial S^{i}}{\partial \theta} \right] d\mu, & \text{when } -\frac{\partial S^{i}}{\partial \theta} > 0, \\ \int_{\mathcal{S}_{i} \cap \mathbb{A}} \left[-\frac{\partial S^{i}}{\partial \theta} \right] d\mu, & \text{when } -\frac{\partial S^{i}}{\partial \theta} < 0. \end{cases}$$

In (56), we are evaluating the integrals for which $-\frac{\partial S^i}{\partial \theta} > 0$ on slightly smaller domains, so we only slightly decrease the contribution of the positive integrals to the sum (55).

Then (55) implies that we can choose $I'_{\alpha} \gtrsim I_{\alpha}$ and $I'_{\beta} \lesssim I_{\beta}$, and $0 < C_2 <$ C_1 , such that

(57)
$$\sum_{i=1}^{L} \mathcal{I}_i > C_2 > 0.$$

Define

(58)
$$T_{\epsilon}(I,\theta) := \sigma_{\epsilon}^{i}(I,\theta) \text{ whenever } (I,\theta + \Delta^{i}(I)) \in \mathcal{S}_{i}, \text{ for } i = 1,\ldots,L.$$

The orbits of T_{ϵ} are in fact pseudo-orbits of the iterated function system generated by $\{\sigma_{\epsilon}^i\}_{i=1,\dots,L}$. We denote such an orbit by

$$(I_n, \theta_n)$$
, for $n = 0, \dots, N$.

We will argue that on each strip S_i , i = 1, ..., L, the change in I resulting from applying the corresponding scattering map σ^i_ϵ , , can be approximated by the integral of $-\frac{\partial S^i}{\partial \theta}$ over that strip. We give the details below.

Let $\epsilon > 0$ be fixed and sufficiently small. We consider the set

$$X_{\epsilon} = \bigcup_{n>0} T_{\epsilon}^{n}(\mathbb{A}'),$$

provided that this set is well-defined in A. See Fig. 6.

In the case when the set X_{ϵ} is not well-defined in \mathbb{A} , it means that there are points $(I_0, \theta_0) \in \mathbb{A}'$ whose orbits leave \mathbb{A} at some moment. In this case, there exist N such that

$$I_0 < I'_{\beta}$$
 and $I_N > I_{\beta}$, or $I_0 > I'_{\alpha}$ and $I_N < I_{\alpha}$.

In either case we obtain a pseudo-orbit that changes the action coordinate by O(1), which proves our claim.

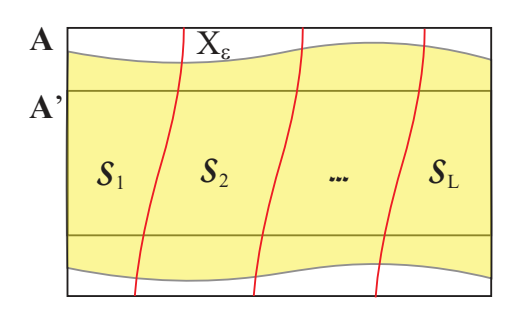


FIGURE 6. The strips S_i , the annuli \mathbb{A} and \mathbb{A}' , and the set X_{ϵ} .

From now on, we assume that X_{ϵ} is a well-defined set in \mathbb{A} . Since $T_{\epsilon}(X_{\epsilon}) \subseteq X_{\epsilon}$, it follows that any orbit $(I_n, \theta_n)_{n \geq 0}$ starting at a point (I_0, θ_0) in X_{ϵ} stays in X_{ϵ} for all future times.

Recall Birkhoff's Ergodic Theorem. If $T: X \to X$ is a measure preserving map, where (X, \mathcal{B}, μ) is a finite measure space, and $f \in L^1(X)$, then

$$\frac{1}{N} \sum_{n=0}^{N-1} f \circ T^n(x) \to \bar{f}(x) \text{ for } \mu - \text{a.e. } x \in X$$

where $\bar{f} \in L^1(X)$ is T-invariant and satisfies

$$\int_{X} \bar{f} d\mu = \int_{X} f d\mu.$$

Moreover, if T is ergodic (i.e., any T-invariant set has either zero or full measure), then the pointwise limit is a constant $\bar{f} = \frac{1}{\mu(X)} \int_X f d\mu$.

We will apply Birkhoff's theorem in the case when $X := X_{\epsilon}$, μ is the Lebesgue measure on \mathbb{A} restricted to X_{ϵ} , and $T := T_{\epsilon}$. We are under the assumption that X_{ϵ} is a well-defined subset of \mathbb{A} , hence of finite measure, and that any pseudo-orbit under T_{ϵ} starting in X_{ϵ} does not leave X_{ϵ} , hence $T_{\epsilon}: X_{\epsilon} \to X_{\epsilon}$ is well-defined. Since each scattering map σ_{ϵ}^{i} , $i = 1, \ldots, L$, is symplectic, the map T_{ϵ} is also symplectic, hence measure preserving.

Define

(59)

$$f_i(I,\theta) := -\frac{\partial S^i}{\partial \theta}(I,\theta + \Delta^i(I))$$
 whenever $(I,\theta + \Delta^i(I)) \in \mathcal{S}^i$, for $i = 1,\ldots,L$.

Applying Birkhoff's theorem to T_{ϵ} and f_i we obtain

$$\frac{1}{N} \sum_{n=0}^{N-1} f_i \circ T_{\epsilon}^n(I_0, \theta_0) \to \bar{f}_i(I_0, \theta_0) \text{ for } \mu - \text{a.e. } (I_0, \theta_0),$$

for some L^1 -function \bar{f}_i , satisfying

$$\int_{X_{\epsilon}} \bar{f}_i d\mu = \int_{X_{\epsilon}} f_i d\mu.$$

Since T_{ϵ} may not be ergodic, when we apply Birkhoff's theorem we obtain a pointwise limit that is in general not a constant but a function.

We have

$$\mathbb{A}' \subset X_{\epsilon} \subset \mathbb{A}$$
.

If
$$-\frac{\partial S^i}{\partial \theta} > 0$$
 on S_i , then

(60)
$$\int_{X_{\epsilon}} \bar{f}_i d\mu \ge \int_{\{(I,\theta) \mid (I,\theta) \in \mathcal{S}_i \cap \mathbb{A}'\}} \left[-\frac{\partial S^i}{\partial \theta} (I, \theta + \Delta^i(I)) \right] dI \wedge d\theta = \mathcal{I}_i.$$

The last equality follows from the change of variable formula.

If $-\frac{\partial S^i}{\partial \theta} < 0$ on S_i , then we similarly obtain

(61)
$$\int_{X_{\epsilon}} \bar{f}_i d\mu \ge \int_{\{(I,\theta) \mid (I,\theta) \in \mathcal{S}_i \cap \mathbb{A}\}} \left[-\frac{\partial S^i}{\partial \theta} (I, \theta + \Delta^i(I)) \right] dI \wedge d\theta = \mathcal{I}_i.$$

In either case,

(62)
$$\int_{X_{\epsilon}} \bar{f}_i d\mu \ge \mathcal{I}_i.$$

For every $\epsilon > 0$ there exists $N_i = N_i(\epsilon)$ such that for $N \geq N_i$ we have

$$\left|\frac{1}{N}\sum_{n=0}^{N-1}\left[-\frac{\partial S^i}{\partial \theta}(I_n,\theta_n+\Delta^i(I_n))\right]\right| = \left|\frac{1}{N}\sum_{n=0}^{N-1}f_i\circ T^n_\epsilon(I_0,\theta_0) - \bar{f}_i\right| < \epsilon,$$

SC

(63)
$$\sum_{n=0}^{N-1} f_i \circ T_{\epsilon}^n(I_0, \theta_0) > N(\bar{f}_i - \epsilon).$$

Whenever a point (I_n, θ_n) of the pseudo-orbit is such that $(I_n, \theta_n + \Delta^i(I_n))$ lands in S_i , the corresponding change in action when moving to the next point of the pseudo-orbit (I_{n+1}, θ_{n+1}) is

$$I_{n+1} - I_n = -\epsilon \frac{\partial S^i}{\partial \theta} (I_n, \theta_n + \Delta^i(I_n)) + O(\epsilon^2).$$

On \mathbb{A} we can uniformly bound each error term by $C_0 \epsilon^2$ for some $C_0 > 0$. Thus, the cumulative change in I associated to the points of the pseudo-orbit that land in \mathcal{S}_i is given by

$$\Sigma_i := \sum_{\substack{n=0,\dots,N-1\\\theta_n + \Delta^i(I_n) \in \mathcal{S}_i}} \left[-\epsilon \frac{\partial S^i}{\partial \theta} (I_n, \theta_n + \Delta^i(I_n)) + O(\epsilon^2) \right].$$

Considering the bounds on the error terms we have

$$\Sigma_i > \epsilon \sum_{n=0}^{N-1} f_i \circ T^n(I_0, \theta_0) - NC\epsilon^2 > \epsilon N(\bar{f}_i - (1 + C_0)\epsilon).$$

Then the cumulative change in I along the pseudo-orbit (I_{n+1}, θ_{n+1}) , for $n = 0, \ldots, N$, where $N \geq \bar{N} = \bar{N}(\epsilon)$, with $\bar{N}(\epsilon)$ sufficiently large, is bounded by

$$\Sigma := \sum_{i=1}^{L} \Sigma_i > \epsilon N(\bar{f} - (1 + C_0)\epsilon),$$

where

$$\bar{f} = \sum_{i=1}^{L} \bar{f}_i.$$

From (62) it follows

$$\int_{X_{\epsilon}} \bar{f} d\mu = \sum_{i=1}^{L} \int_{X_{\epsilon}} \bar{f}_i \ge \sum_{i=1}^{L} \mathcal{I}_i \ge C_2 > 0.$$

This implies that

$$\mu\{(I,\theta) \mid \bar{f}(I,\theta) \ge C_2/\mu(X_{\epsilon})\} > 0.$$

Since $C_2/\mu(X_{\epsilon}) \geq C_2/\mu(\mathbb{A}) > 0$, then for $C_3 = C_2/\mu(\mathbb{A})$, which is independent of ϵ , we have that there exists a positive measure set \mathcal{D} of points (I_0, θ_0) such that

$$\bar{f}(I_0, \theta_0) > C_3 > 0.$$

For points $(I_0, \theta_0) \in \mathcal{D}$ we have

$$\Sigma := \sum_{i=1}^{L} \Sigma_i > \epsilon N(C_3 - (1 + C_0)\epsilon) > \epsilon NC_4,$$

for some $0 < C_4 \lesssim C_3$ independent of ϵ . The last inequality holds whenever ϵ is sufficiently small with respect to C_3 . Since this holds for N large enough, we can choose $N > 1/\epsilon$, and we conclude that

$$\Sigma > C_4 > 0.$$

That is, there exists a positive measure set \mathcal{D} of points (I_0, θ_0) in X_{ϵ} such that the change in I along the corresponding pseudo-orbit $(I_n, \theta_n)_{n=0,\dots,N}$ is at least $C_4 > 0$.

Remark 5.8. It is well known that for general ergodic dynamical systems, the rate of convergence of the Birkhoff sums can be arbitrarily slow, as shown in [Kre78]. Even for a rigid rotation of the circle, estimating the convergence rate is non-trivial, as it depends on continued fraction expansion of the rotation number; a related result is the Denjoy-Koksma's inequality [Her79]. Therefore, in the above argument we may need to choose N very large. This approach does not immediately lead to estimates for the diffusion time. It may be possible that by using weighted Birkhoff averaging methods one can obtain fast convergence and time estimates [DY18, DSSY17].

Remark 5.9. Proposition 5.7 only says that there is a pseudo-orbit along which I changes by O(1), but it does not say whether I increases or decreases along that pseudo-orbit. If we have more information on the scattering maps, we can also obtain the existence of pseudo-orbits along which I increases (decreases) by O(1). See Section 6.4.

6. Numerical verification of the conditions in Theorem 5.1

In Sections 6.1, 6.2, 6.3 we verify numerically the conditions (i)-(v) in Theorem 5.1. That is, we establish numerically the existence of transverse homoclinic and heteroclinic connections to the NHIM's Λ_0^1 and of heteroclinic connections between Λ_0^1 and Λ_0^2 for the unperturbed system, we compute the unperturbed scattering map associated to homoclinic/heteroclinic connections, and then we compute the effect of the perturbation on these maps. In Section 6.4 we verify numerically the condition (vi) in Theorem 5.1, which amounts to verifying Proposition 5.7. The conclusion of this section is the existence of diffusing orbits along which energy grows by O(1).

6.1. Homoclinic and heteroclinic connections to the unperturbed NHIM's.

6.1.1. Lyapunov orbits. We compute the NHIM's Λ_0^1 near L_1 , for the energy range

$$[h_{\alpha}, h_{\beta}] = [-2.10446079, -2.07715457]$$

The corresponding range for $x^*(h)$ is $[x^*(h_{\beta}), x^*(h_{\alpha})] = [0.615, 0.63]$. In Table 1, we give the energy levels, the initial conditions and the periods for a family of periodic orbits with $x^*(h)$ within this range. The corresponding periodic orbits are shown in Fig. 7.

h	$\pm x^*(h)$	$\pm p_y(h)$	T(h)
-2.07715457	± 0.615	± 0.48123483	3.05967299
-2.08671819	± 0.62	± 0.45248801	3.05678890
-2.09582648	± 0.625	± 0.42353750	3.05406407
-2.10446079	± 0.63	± 0.39437305	3.05150060

Table 1. Initial conditions, periods and energy levels of the Lyapunov periodic orbits shown in Fig. 7.

6.1.2. Homoclinic connections. We compute the stable and unstable manifolds, $W^s(\lambda_1(h))$ and $W^u(\lambda_1(h))$, respectively, associated to the Lyapunov orbits $\lambda_1(h)$, for $h \in [h_\alpha, h_\beta]$. As an example, we show the projections of the stable and unstable manifolds of the Lyapunov orbit corresponding to $x^*(h_\alpha) = 0.63$, onto the (x, y, p_x) -coordinates, (x, y)-coordinates, and (x, p_x) coordinates in Fig. 8.

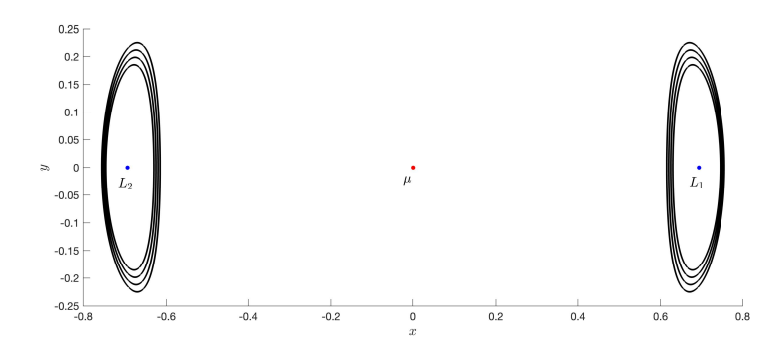


FIGURE 7. Families of periodic Lyapunov orbits emanating from L_1 and L_2 for $|x^*(h)| \in [0.615, 0.63]$.

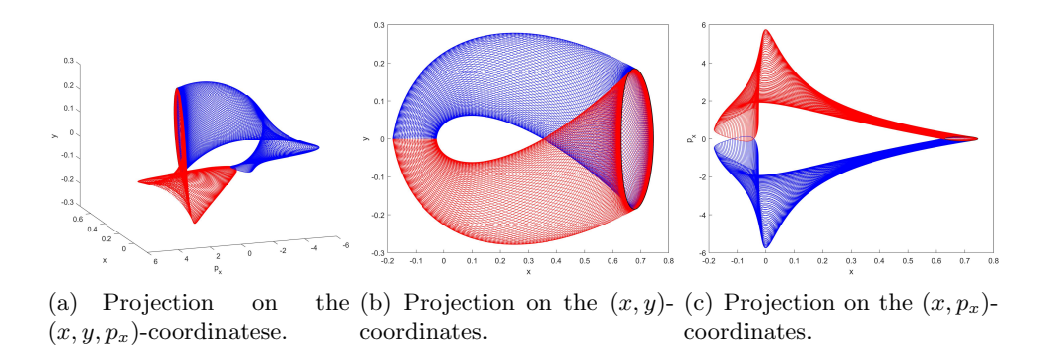


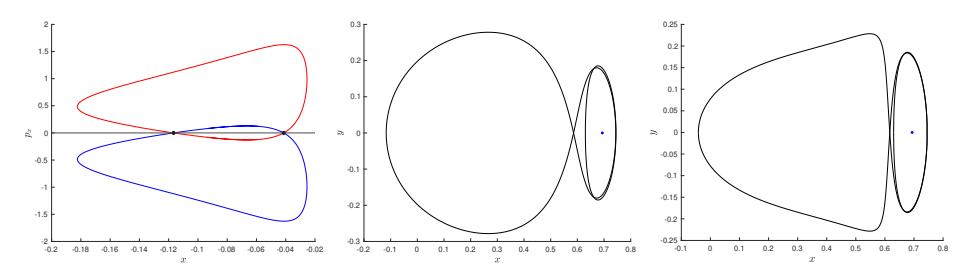
FIGURE 8. Stable (red) and unstable (blue) manifold of the Lyapunov periodic orbit for $x^*(h_\alpha) = 0.63$.

The manifolds are computed up to the their first intersections with the section $\Sigma = \{y = 0, p_y < 0\}$. On this section, we can find transverse homoclinic points as intersection between the stable and unstable manifold cuts with the section Σ . For example, the intersections of the stable and unstable manifold associated with the periodic orbit corresponding to $x^*(h_\alpha) = 0.63$ are shown in Fig. 9. Note that there are two homoclinic points, z_1 and z_2 (given explicitly in Table 2 and Table 3 for $x(h_\alpha) = 0.63$), which give rise to two homoclinic orbits that are shown in Fig. 9.

6.1.3. Heteroclinic connections. For studying the heteroclinic connections between Λ_0^1 and Λ_0^2 , we consider the same energy range $[h_{\alpha}, h_{\beta}]$ given in (64).

The corresponding range for $x^*(h)$ is $[x_1^*(h_\beta), x_1^*(h_\alpha)] = [0.615, 0.63]$ and $[x_2^*(h_\alpha), x_2^*(h_\beta)] = [-0.63, -0.615]$, with the positive sign corresponding to L_1 and the negative sign to L_2 .

In Table 1, we give the energy levels, initial conditions and periods of the families of Lyapunov periodic orbits. The corresponding periodic orbits are shown in Fig. 7.



(a) Homoclinic points z_2 (on (b) Homoclinic orbit $\Phi_0^t(z_2)$. (c) Homoclinic orbit $\Phi_0^t(z_1)$. the left) and z_1 (on the right).

FIGURE 9. Homoclinic points and orbits.

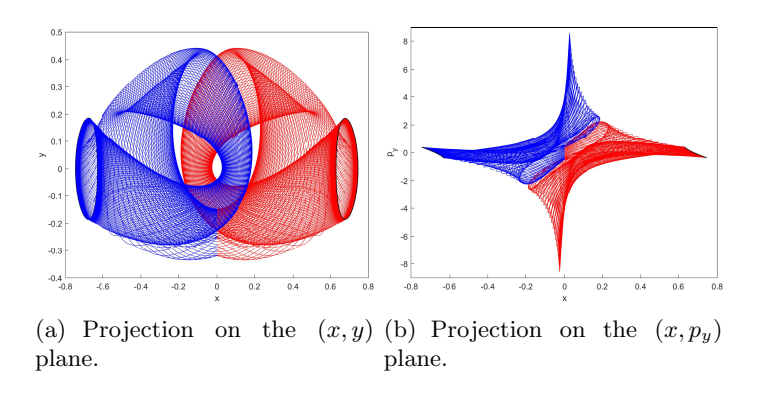


FIGURE 10. Stable manifold (red) of the Lyapunov periodic orbit that start at $x_1^*(h_\alpha) = 0.63$ and unstable manifold (blue) of the Lyapunov periodic orbit that start at $x_2^*(h_\alpha) = -0.63$.

Then we compute the stable and unstable manifolds, $W^s(\lambda_1(h))$ and $W^u(\lambda_2(h))$ associated to Lyapunov orbits $\lambda_1(h)$ and $\lambda_2(h)$, respectively, for $h \in [h_\alpha, h_\beta]$. As an example, we show the projection of the stable manifold of the Lyapunov periodic orbit that start at $x_1^*(h_\alpha) = 0.63$ and unstable manifold of the Lyapunov periodic orbit that start at $x_2^*(h_\alpha) = -0.63$, onto the (x, y)-coordinates, and (x, p_x) coordinates in Fig. 10.

The manifolds are computed up to the their second intersection with the section $\Sigma = \{x = 0, p_x > 0\}$. On this section, we can find a transverse intersection between the stable and unstable manifold, then we obtain two heteroclinic points, z_1 and z_2 , from which two heteroclinic orbits are obtained. See Fig. 11. Due to the symmetry $S(x, y, p_x, p_y, t) = (x, -y, -p_x, p_y, -t)$ there are also a symmetric heteroclinic connections given by the intersection of $W^u(\lambda_1(h))$ and $W^s(\lambda_2(h))$. The corresponding heteroclinic points \hat{z}_1, \hat{z}_2

right).

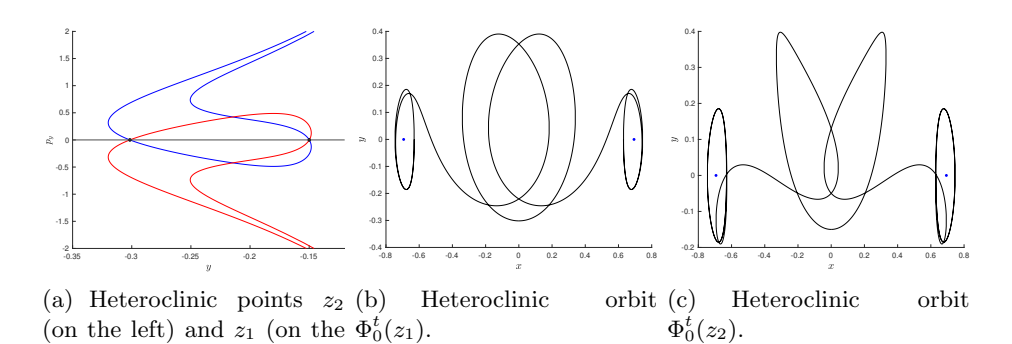


FIGURE 11. Heteroclinic points and orbits.

are the symmetric images under S of z_1, z_2 , respectively. These heteroclinic points are given explicitly in Table 6 and 7.

6.2. The unperturbed scattering map associated to homoclinic and heteroclinic connections.

6.2.1. The unperturbed scattering map associated to homoclinic connections. Consider the homoclinic points $z_i = z_i(h)$, i = 1, 2, defined in Section 6.1.2, for the corresponding energy range $h \in [h_\alpha, h_\beta]$. For each homoclinic point z_i , let $z_i^+ \in \Lambda_0^1$ be the foot-point of the stable fiber through z_i , and $z_i^- \in \Lambda_0^1$ be the foot-point of the unstable fiber through z_i . In (I, θ) -coordinates, $z_i^+ = k_0(I_i, \theta_i^+)$ and $z_i^- = k_0(I_i, \theta_i^-)$.

A sample of homoclinic points $z_i = z_i(h)$ and the corresponding values of $x^*(h)$ for the considered energy range are given in Table 2 and Table 3, and shown in Fig. 12. The corresponding values θ_i^{\pm} are given in Table 2 and Table 3. Finally, the points z_i^{\pm} are given in Table 4 and 5. Note that, $z_i^{\pm} \approx (x^*(h), 0, 0, p_u(h))$.

Consider the homoclinic channel given by

(65)
$$\Gamma_{\text{hom}}^{i} = \bigcup_{\substack{h \in [h_{\alpha}, h_{\beta}] \\ \theta \in [\theta_{i}^{-}, 1 + \theta_{i}^{-}]}} \Phi^{(\theta - \theta_{i}^{-})T}(z_{i}(h)).$$

The associated scattering maps in (I, θ) -coordinates are the phase-shift given by

$$\sigma_0^i(I,\theta) = (I,\theta + (\theta_i^+ - \theta_i^-)), \text{ for } i = 1, 2.$$

(As in Section 5.4, we identify a scattering map σ_0^i with its representation s_0^i in the action-angle coordinates.) By the symmetry $S(x,y,\dot{x},\dot{y},t)=(x,-y,-\dot{x},\dot{y},-t)$ we have $\theta_i^+=-\theta_i^-$, then

(66)
$$\sigma_0^i(I,\theta) = (I,\theta + \Delta^i), \text{ where } \Delta^i = \theta_i^+ - \theta_i^- = -2\theta_i^-.$$

$x^*(h)$	$z_1(h)$	$\theta_1^{\pm}(h)$
0.615	(-0.14646739, 0, 0, -3.09272039)	± 2.27849625
0.62	(-0.13707337, 0, 0, -3.23629663)	± 2.28369125
0.625	(-0.12723761, 0, 0, -3.40227909)	± 2.29106293
0.63	(-0.11666113, 0, 0, -3.60215892)	± 2.30161988

Table 2. Homoclinic point z_1 and θ_1^{\pm} .

x^*	(h)	$z_2(h)$	$\theta_2^{\pm}(h)$
0.	615	(-0.02675921, 0, 0, -8.40169252)	± 2.49677491
0.	62	(-0.03085457, 0, 0, -7.78778643)	± 2.48835256
0.	625	(-0.03563430, 0, 0, -7.20679133)	± 2.47799047
0.	63	(-0.04141244, 0, 0, -6.64009686)	± 2.46465922

Table 3. Homoclinic point z_2 and θ_2^{\pm} .

$x^*(h)$	$z_1^{\pm}(h)$
0.615	$(0.61500027, \mp 0.00000005, \mp 0.00000100, 0.48123436)$
0.62	$(0.62000004, \mp 0.00000011, \mp 0.00000028, 0.45248794)$
0.625	$(0.62500023, \mp 0.00000006, \mp 0.00000083, 0.42353712)$
0.63	$(0.63000040, \mp 0.00000000, \pm 0.00000132, 0.39437240)$

Table 4. Footpoints z_1^{\pm} of the homoclinic point z_1 .

$x^*(h)$	$z_2^{\pm}(h)$
0.615	$(0.61499366, \pm 0.00000076, \pm 0.00001982, 0.48124537)$
0.62	$(0.61999254, \pm 0.00000079, \pm 0.00002317, 0.45250024)$
0.625	$(0.62499943, \mp 0.00000216, \pm 0.0000008, 0.42353842)$
0.63	$(0.63000023, \pm 0.00000018, \pm 0.0000008, 0.39437267)$

TABLE 5. Footpoints z_2^{\pm} of the homoclinic point z_2 .

6.2.2. The unperturbed scattering map associated to heteroclinic connections in the CH4BP. Consider now a heteroclinic point $z_i = z_i(h)$, i = 1, 2 defined in Section 6.1.3, for the corresponding energy range $h \in [h_{\alpha}, h_{\beta}]$. Consider the heteroclinic channel

(67)
$$\Gamma_{\text{het}}^{i} = \bigcup_{\substack{h \in [h_{\alpha}, h_{\beta}] \\ \theta \in [\theta_{i}^{-}, 1 + \theta_{i}^{-}]}} \Phi^{(\theta - \theta_{i}^{-})T}(z_{i}).$$

This heteroclinic channel is represented in Fig. 15.

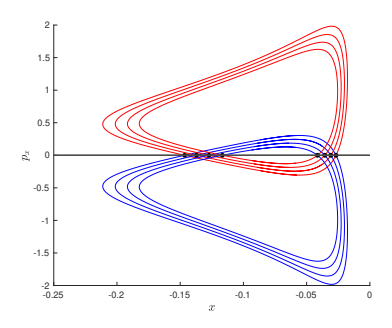


FIGURE 12. Homoclinic point z_2 (on the left) and z_1 (on the right) for $x^*(h) = 0.615, 0.62, 0.625, 0.63$.

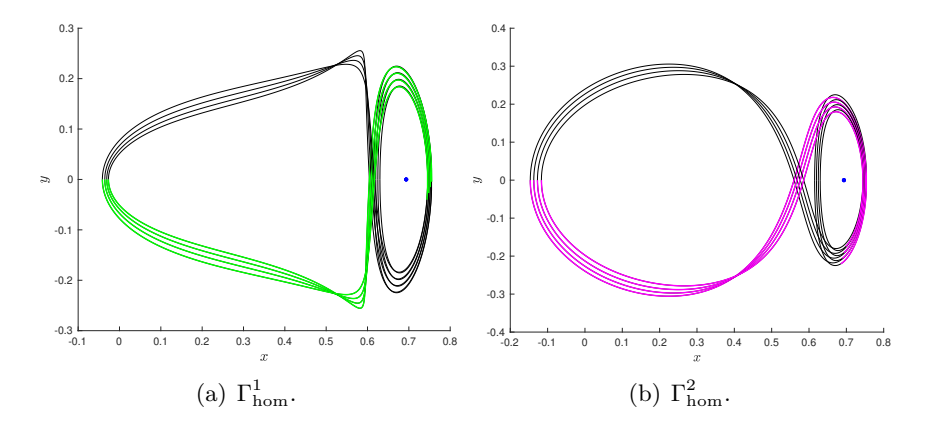


FIGURE 13. Homoclinic channels Γ_{hom}^1 and Γ_{hom}^2 .

A sample of heteroclinic points z_i , \hat{z}_i and the corresponding values of x^* for the considered energy range are given in the Table 7. The corresponding values θ_i^{\pm} and z_i^{\pm} are given in Tables 6 and 7. The associated scattering map in (I, θ) -coordinates is a phase-shift given

by

$$\sigma_0^i(I,\theta) = (I,\theta + (\theta_i^+ - \theta_i^-)).$$

Since, by the symmetry $S'(x,y,\dot{x},\dot{y},t)=(-x,y,\dot{x},-\dot{y},-t)$ we have $\theta_i^+=$ $-\theta_i^-$, we have

(68)
$$\sigma_0^i(I,\theta) = (I,\theta + \Delta^i), \text{ where } \Delta^i = \theta_i^+ - \theta_i^- = -2\theta_i^-.$$

6.3. Perturbed scattering map associated to homoclinic and heteroclinic connections.

6.3.1. Perturbed scattering map associated to homoclinic connections. Consider the homoclinic channel Γ_{hom}^{i} defined by (65). For the energy range $[h_{\alpha}, h_{\beta}]$ we compute the Hamiltonian S^{i} that generates the scattering map σ_{ϵ}^{i} associated to the homoclinic point z_{i} , in the (non-symplectic) coordinates

$x^*(h)$	$z_1(h), \hat{z}_1(h)$	$\theta_2^{\pm}(h)$
0.615	$(0, \mp 0.32513154, \pm 1.413249476243125, 0)$	± 2.56696772
0.62	$(0, \mp 0.31736214, \pm 1.459016313792567, 0))$	± 2.55400246
0.625	$(0, \mp 0.30951753, \pm 1.506725576126874, 0)$	± 2.54075381
0.63	$(0, \pm 0.30157444, \pm 1.55664227, 0)$	± 2.52702772

Table 6. Heteroclinic points z_1, \hat{z}_1 and θ_1^{\pm} .

$x^*(h)$	$z_2(h),\hat{z}_2(h)$	$\theta_1^{\pm}(h)$
0.615	$(0, \mp 0.13480207, \pm 3.26837828, 0)$	± 2.04588521
0.62	$(0, \mp 0.13957356, \pm 3.18684274, 0)$	± 2.05160310
0.625	$(0, \mp 0.14460595, \pm 3.10468687, 0)$	± 2.05811547
0.63	$(0, \mp 0.14991892, \pm 3.02186543, 0)$	± 2.06560153

Table 7. Heteroclinic points z_2, \hat{z}_2 and θ_2^{\pm} .

$x^*(h)$	$z_1^{\pm}(h)$
0.615	$(\pm 0.61500108, 0.00000001, 0.00000360, \pm 0.48123302)$
0.62	$(\pm 0.62000004, 0.00000010, 0.000000045, \pm 0.45248793)$
0.625	$(\pm 0.62500059, 0.00000015, 0.00000215, \pm 0.42353653)$
0.63	$(\mp 0.63000045, 0.00000009, 0.00000163, \mp 0.39437232)$

Table 8. Footpoints z_1^{\pm} of the heteroclinic point z_1 .

$x^*(h)$	$z_2^{\pm}(h)$
0.615	$(\pm 0.61499894, -0.00000004, 0.00000329, \pm 0.48123659)$
0.62	$(\pm 0.61999901, -0.00000003, 0.00000316, \pm 0.45248962)$
0.625	$(\pm 0.62499909, -0.000000000, 0.00000300, \pm 0.42353896)$
0.63	$(\pm 0.62999918, -0.00000002, 0.00000285, \pm 0.39437436)$

Table 9. Footpoints z_2^{\pm} of the heteroclinic point z_2 .

 $(x^*(h), \theta)$. To exclude possible failure of monodromy of the scattering map, we restrict $\theta \in [0, 1)$.

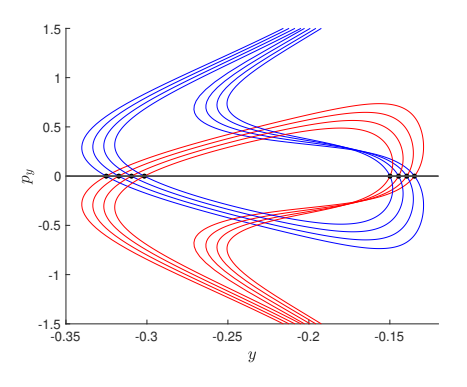


FIGURE 14. Heteroclinic point z_2 (on the left) and z_1 (on the right) for $x^*(h) = 0.615, 0.62, 0.625, 0.63$.

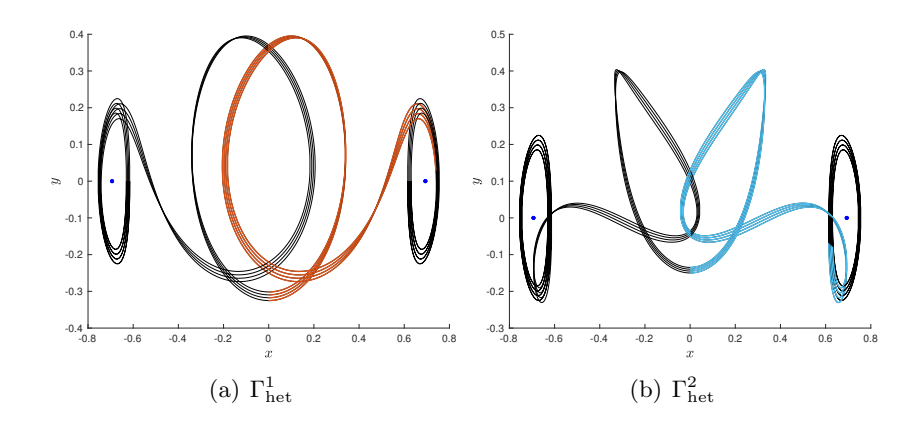


Figure 15. Heteroclinic channels $\Gamma^1_{\rm het}$ and $\Gamma^2_{\rm het}$.

Using (43) we can write

(69)
$$S^{i}(x^{*}, \theta, s) = \int_{-\infty}^{0} \left[G(\Phi_{0}^{t} \circ \Phi_{0}^{(\theta + \theta_{i}^{-})T}(z_{i}), s + t)) - G(\Phi_{0}^{t}(k_{0}(x^{*}, \theta + 2\theta_{i}^{-})), s + t) \right] dt + \int_{0}^{+\infty} \left[G(\Phi_{0}^{t} \circ \Phi_{0}^{(\theta + \theta_{i}^{-})T}(z_{i}), s + t) - G(\Phi_{0}^{t}(k_{0}(x^{*}, \theta)), s + t) \right] dt.$$

For $s = \pi/2$ we obtain the explicit formula

(70)
$$S^{i}(x^{*}, \theta, \pi/2) = -\int_{0}^{\infty} \sin(t) \left[H_{1} \left(\Phi_{0}^{t+(\theta+\theta_{i}^{-})T(x^{*})}(z_{i}) \right) - H_{1} \left(\Phi_{0}^{t+(\theta+\theta_{i}^{-})T(x^{*})}(k_{0}(x^{*}, \theta_{i}^{+})) \right) \right] dt$$
$$- \int_{-\infty}^{0} \sin(t) \left[H_{1} \left(\Phi_{0}^{t+(\theta+\theta_{i}^{-})T(x^{*})}(z_{i}) \right) - H_{1} \left(\Phi_{0}^{t+(\theta+\theta_{i}^{-})T(x^{*})}(k_{0}(x^{*}, \theta_{i}^{-})) \right) \right] dt$$

For brevity, we denote this by $S^{i}(x^{*}, \theta)$.

We stress that the explicit formula (70) is the formally the same for both homoclinic and heteroclinic connections.

For a range $x^* = x^*(h) \in [0.615, 0.63]$ we show the 3D-plot and the contour plot of the function

$$(x^*, \theta) \mapsto S^i(x^*, \theta)$$

in Fig. 16. The contour plot represents the level sets of the Hamiltonian S^i in terms of the (non-symplectic) coordinates (x^*, θ) . We notice the presence of elliptic and saddle fixed points, elliptic islands, and separatrices that organize the phase space of the NHIM.

We compute $-\frac{\partial S^i}{\partial \theta}(I, \theta + \Delta^i(I))$, for i = 1, 2, which follows from (44), and we plot it in Fig. 17.

In Fig. 16 and Fig. 17 we can identify domains where the scattering map yields the largest growth/decay in the action, as well as the portions where the scattering map yields the smallest change. We note that, due to the angle-shift in $-\frac{\partial S^i}{\partial \theta}(I, \theta + \Delta^i(I))$, applying the scattering map σ^i_{ϵ} to a point (I, θ) amounts to taking a step in the angle direction from (I, θ) to $(I, \theta + \Delta^i(I))$, and then taking a step of size ϵ along the contour plot of S^i through $(I, \theta + \Delta^i(I))$, plus a small error $O(\epsilon^2)$.

6.3.2. Perturbed scattering map associated to heteroclinic connections. Consider the heteroclinic connection $W^u(\Lambda_0^2) \cap W^s(\Lambda_0^1)$, and the heteroclinic channels Γ^i_{het} given by (67), for i=1,2. For each scattering map σ^i_{ϵ} , the corresponding generating Hamiltonian S^i is given by the formula (70), where in the case of heteroclinic connection z_i refers to a heteroclinic point in $W^u(\Lambda_0^2) \cap W^s(\Lambda_0^1)$, and the θ refers to the action-angle coordinate system associated to Λ_0^2 .

As in the case of homoclinic connections, for the range $x^* \in [0.615, 0.63]$, we show the 3D-plot and the contour plot of the function

$$(x^*, \theta) \mapsto S^i(x^*, \theta)$$

in Fig. 18 (as before, we dropped $\pi/2$ from the notation). The contour plot represents the level sets of the Hamiltonian S^i in terms of the (non-symplectic) coordinates (x^*, θ) . Again, we notice the presence of elliptic and

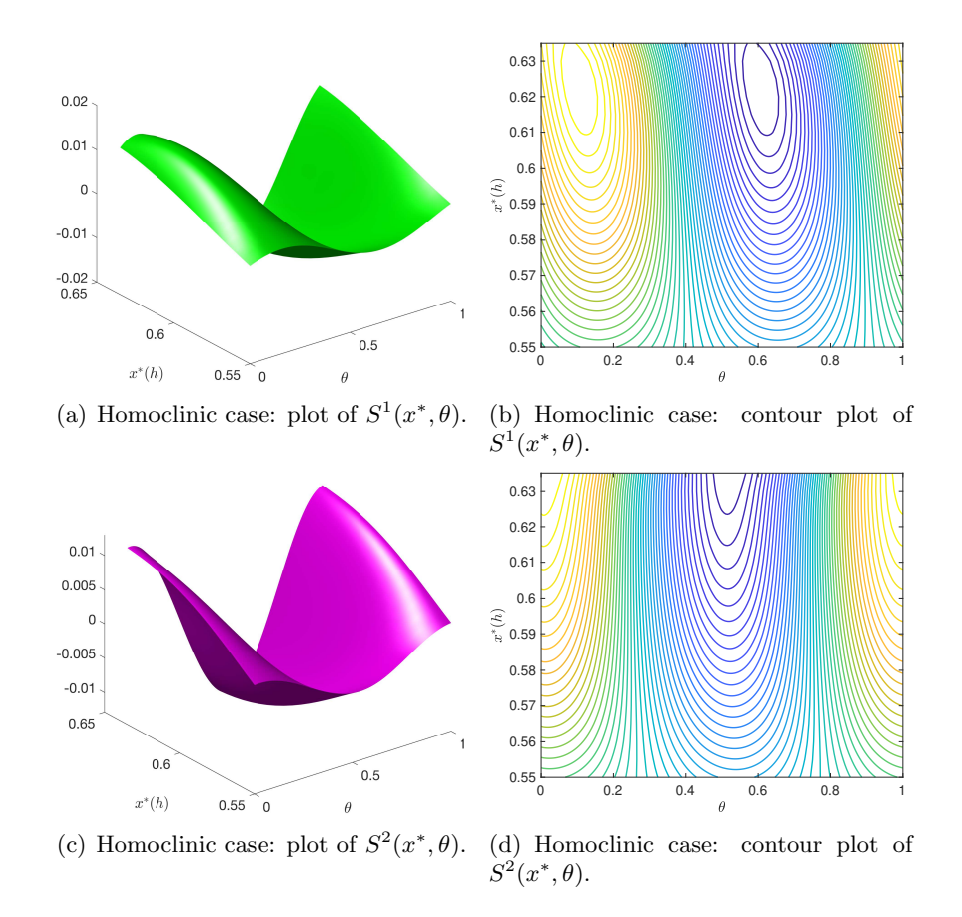


FIGURE 16. Homoclinic case: 3D-plot and contour plot of $S^{i}(x^{*},\theta), h \in [h_{\alpha},h_{\beta}], x^{*} \in [0.615,0.63], \text{ and } \theta \in [0,1).$

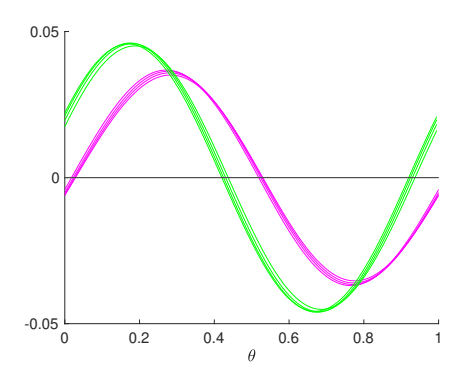
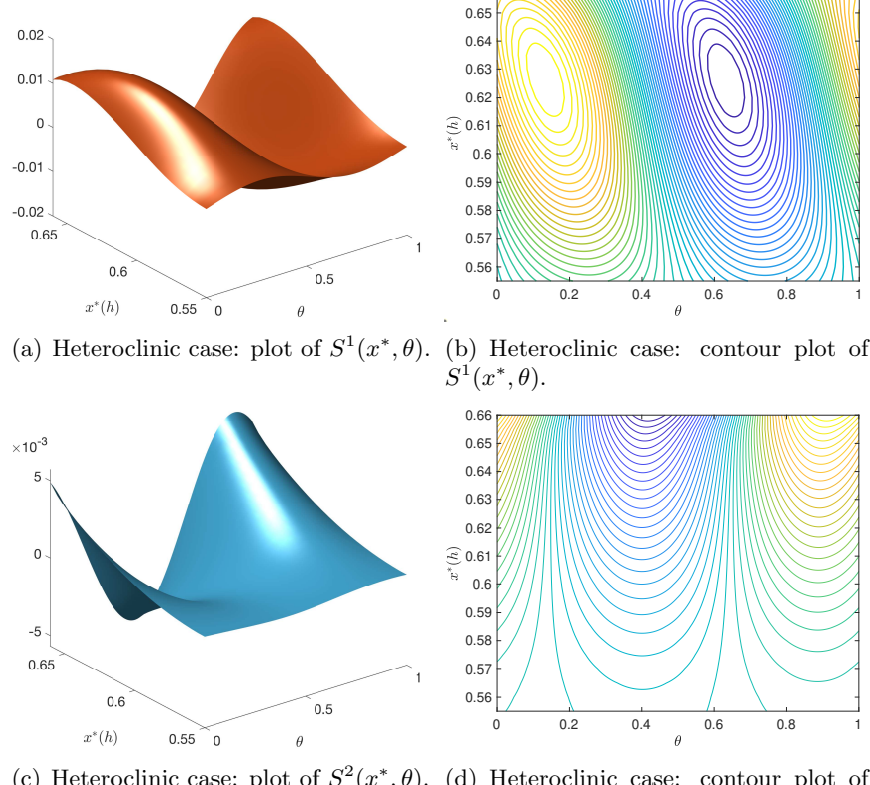


Figure 17. Homoclinic case: plot of $-\frac{\partial S^i}{\partial \theta}(I, \theta + \Delta^i(I)), i = 1, 2.$

saddle fixed points, elliptic islands, and separatrices that organize the phase space of the NHIM Λ_0^2 .



(c) Heteroclinic case: plot of $S^2(x^*, \theta)$. (d) Heteroclinic case: contour plot of $S^2(x^*,\theta).$

FIGURE 18. Heteroclinic case: 3D-plot and contour plot of $S^{i}(x^{*}, \theta), h \in [h_{\alpha}, h_{\beta}], x^{*} \in [0.615, 0.63], \text{ and } \theta \in [0, 1).$

We plot $-\frac{\partial S^i}{\partial \theta}(I, \theta + \Delta^i(I))$, for i = 1, 2, in Fig. 19. Because of the symmetry $S(x, y, \dot{x}, \dot{y}, t) = (x, -y, -\dot{x}, \dot{y}, -t)$, we also have a heteroclinic connection $W^u(\Lambda_0^1) \cap W^s(\Lambda_0^2)$, with heteroclinic channels $\hat{\Gamma}_{het}^i$ given by (67), for i = 1, 2. The scattering map $\hat{\sigma}_{\epsilon}^{i}$ has the corresponding generating Hamiltonian \hat{S}^i given by the formula (70), where θ refers to the action-angle coordinate system associated to Λ_0^1 . The expression of the scattering map $\hat{\sigma}^i_{\epsilon}$ in the action-angle coordinates on Λ^1_0 is the same as the expression of the scattering map σ^i_ϵ in the action-angle coordinates on Λ_0^2 , and the corresponding generating Hamiltonian \hat{S}^i and S^i are given by identical formulas.

Thus, one can travel along the heteroclinic connection $W^u(\Lambda_0^2) \cap W^s(\Lambda_0^1)$, by using one of the scattering maps σ_{ϵ}^1 , σ_{ϵ}^2 , and then then travel along the heteroclinic connection $W^u(\Lambda_0^1) \cap W^s(\Lambda_0^2)$ by using one of the scattering maps $\hat{\sigma}_{\epsilon}^{1}$, $\hat{\sigma}_{\epsilon}^{2}$. By the symmetry, this is equivalent to applying the scattering maps σ_{ϵ}^{1} , σ_{ϵ}^{2} repeatedly, in any order.

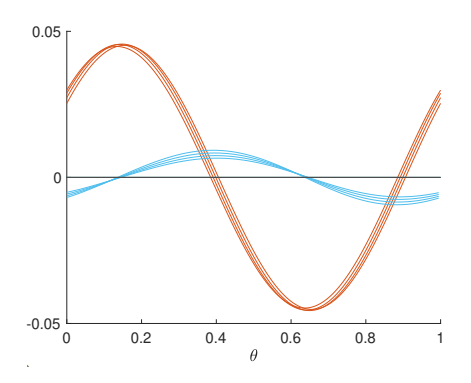


FIGURE 19. Heteroclinic case: plot of $-\frac{\partial S^i}{\partial \theta}(I, \theta + \Delta^i(I)), i = 1, 2.$

6.4. **Proof of Theorem 5.1.** In both the homoclinic case and the heteroclinic case, we have computed two scattering maps of the form

(71)
$$\begin{aligned} \sigma_{\epsilon}^{1}(I,\theta) = & (I,\theta + \Delta^{1}(I)) + \epsilon \left(-\frac{\partial S^{1}}{\partial \theta}, \frac{\partial S^{1}}{\partial I} \right) (I,\theta + \Delta^{1}(I)) + O(\epsilon^{2}), \\ \sigma_{\epsilon}^{2}(I,\theta) = & (I,\theta + \Delta^{2}(I)) + \epsilon \left(-\frac{\partial S^{2}}{\partial \theta}, \frac{\partial S^{2}}{\partial I} \right) (I,\theta + \Delta^{2}(I)) + O(\epsilon^{2}), \end{aligned}$$

for I within some range of the action variable $[I_{\alpha}, I_{\beta}]$.

To obtain diffusing orbits, we will apply Proposition 5.7.

We will consider the case of homoclinic connections and the case of heteroclinic connections at the same time.

We note that the direct application of Proposition 5.7 leads to pseudoorbits for which the action changes by O(1), not that it necessarily increases by O(1). To obtain pseudo-orbits for which the action increases by O(1), we will use the symmetries of the problem.

For each $I \in [I_{\alpha}, I_{\beta}]$ we identify angles A(I), B(I), C(I), D(I) such that

(1) for all $\theta \in [0, A(I)]$, we have:

$$-\frac{\partial S^1}{\partial \theta}(I,\theta+\Delta^1(I)) \geq 0 \text{ and } -\frac{\partial S^1}{\partial \theta}(I,\theta+\Delta^1(I)) \geq -\frac{\partial S^2}{\partial \theta}(I,\theta+\Delta^2(I));$$

(2) for all $\theta \in [A(I), B(I)]$ we have:

$$-\frac{\partial S^2}{\partial \theta}(I, \theta + \Delta^2(I)) \ge 0 \text{ and } -\frac{\partial S^2}{\partial \theta}(I, \theta + \Delta^2(I)) \ge -\frac{\partial S^1}{\partial \theta}(I, \theta + \Delta^1(I));$$

(3) for all $\theta \in [B(I), C(I)]$ we have:

$$-\frac{\partial S^2}{\partial \theta}(I,\theta+\Delta^2(I)) \leq 0 \text{ and } -\frac{\partial S^2}{\partial \theta}(I,\theta+\Delta^2(I)) \geq -\frac{\partial S^1}{\partial \theta}(I,\theta+\Delta^1(I));$$

(4) for all $\theta \in [C(I), D(I)]$ we have:

$$-\frac{\partial S^1}{\partial \theta}(I,\theta+\Delta^1(I)) \leq 0 \text{ and } -\frac{\partial S^1}{\partial \theta}(I,\theta+\Delta^1(I)) \geq -\frac{\partial S^2}{\partial \theta}(I,\theta+\Delta^2(I));$$

	$x^*(h)$	$A(x^*(h))$	$B(x^*(h))$	$C(x^*(h))$	$D(x^*(h))$
(0.615	0.28132387	0.52967673	0.78003687	0.92011641
(0.62	0.28321770	0.52734711	0.78198690	0.92459880
(0.625	0.28497921	0.52391183	0.78380023	0.93003525
(0.63	0.28661829	0.51886508	0.78548687	0.93693844

TABLE 10. The value of $A(x^*(h))$, $B(x^*(h))$, $C(x^*(h))$ and $D(x^*(h))$ for the homoclinic case.

x^*	(h)	$A(x^*(h))$	$B(x^*(h))$	$C(x^*(h))$	$D(x^*(h))$
0.6	615	0.36202487	0.64603186	0.86214616	0.88520444
0.6	52	0.36599741	0.64345707	0.86601010	0.89193879
0.6	525	0.36969259	0.640467541	0.86960783	0.89880348
0.6	63	0.37311753	0.63697309	0.87294588	0.90589438

TABLE 11. The value of $A(x^*(h))$, $B(x^*(h))$, $C(x^*(h))$ and $D(x^*(h))$ for the heteroclinic case.

(5) for all $\theta \in [D(I), 1]$ we have:

$$-\frac{\partial S^1}{\partial \theta}(I,\theta+\Delta^1(I)) \geq 0 \text{ and } -\frac{\partial S^1}{\partial \theta}(I,\theta+\Delta^1(I)) \geq -\frac{\partial S^2}{\partial \theta}(I,\theta+\Delta^2(I)).$$

The values A(I), B(I), C(I), D(I) determine curves in A that divide it into strips:

(72)
$$S_{1} = \{(I, \theta) \in \mathbb{A} \mid \theta \in [0, A(I)]\},$$

$$S_{2} = \{(I, \theta) \in \mathbb{A} \mid \theta \in [A(I), B(I)]\},$$

$$S_{3} = \{(I, \theta) \in \mathbb{A} \mid \theta \in [B(I), C(I)]\},$$

$$S_{4} = \{(I, \theta) \in \mathbb{A} \mid \theta \in [C(I), D(I)]\},$$

$$S_{5} = \{(I, \theta) \in \mathbb{A} \mid \theta \in [D(I), 1]\},$$

The values of A, B, C, D for the homoclinic case are shown in Table 10, and for the heteroclinic case in Table 11.

As in Proposition 5.7, to obtain diffusing orbits we consider pseudo-orbits of the form

(73)
$$(\sigma_{\epsilon}^{i_n} \circ \ldots \circ \sigma_{\epsilon}^{i_1})(I_0, \theta_0), \text{ for } i_1, \ldots, i_n \in \{1, 2\},$$

given by successive applications of σ_{ϵ}^1 or σ_{ϵ}^2 according to the following rules:

- (1) if $(I, \theta + \Delta^1(I)) \in \mathcal{S}_1$ we apply $\sigma_{\epsilon}^1(I, \theta)$; (2) if $(I, \theta + \Delta^2(I)) \in \mathcal{S}_2$ we apply $\sigma_{\epsilon}^2(I, \theta)$; (3) if $(I, \theta + \Delta^2(I)) \in \mathcal{S}_3$ we apply $\sigma_{\epsilon}^2(I, \theta)$; (4) if $(I, \theta + \Delta^1(I)) \in \mathcal{S}_4$ we apply $\sigma_{\epsilon}^1(I, \theta)$; (5) if $(I, \theta + \Delta^1(I)) \in \mathcal{S}_5$ we apply $\sigma_{\epsilon}^1(I, \theta)$.

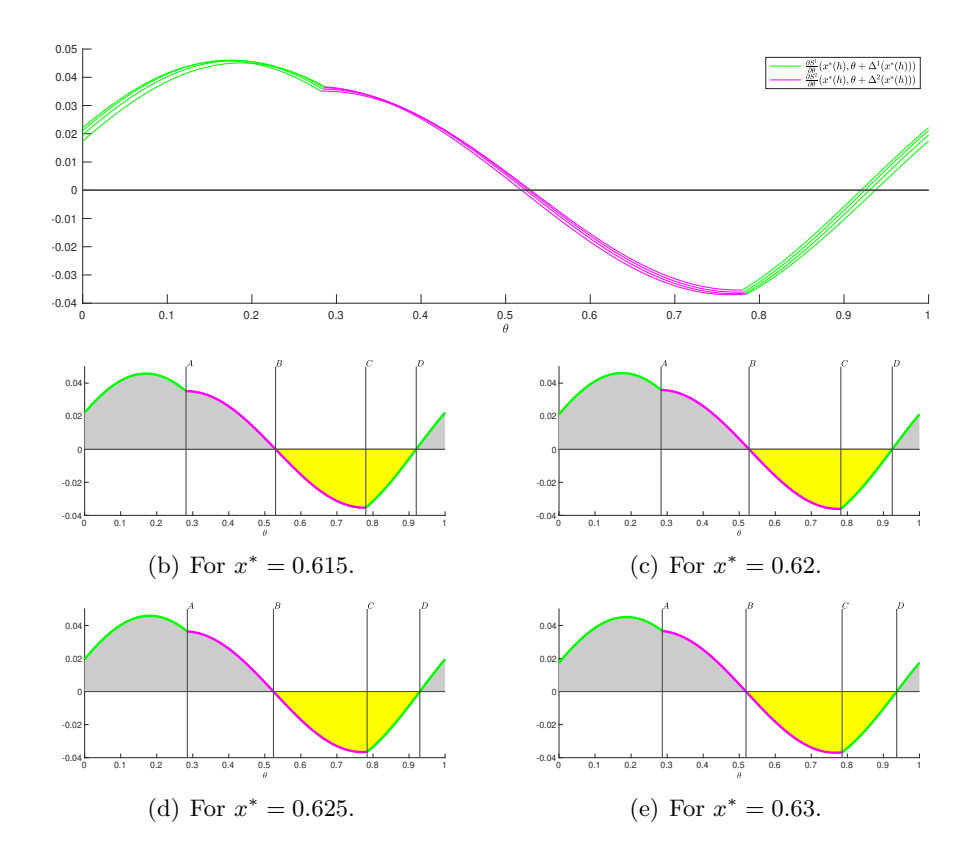


FIGURE 20. Homoclinic connections.

That is, on each strip S_i , i = 1, ..., 5, we select the scattering map $\sigma_{\epsilon}^{\varsigma(i)}$ that yields the maximum growth in the action variable, or the minimum loss in the action variable. We display the corresponding $-\frac{\partial S^{\varsigma(i)}}{\partial \theta}(I, \theta + \Delta^{\varsigma(i)}(I))$ for the homoclinic case in Fig. 20, and for the heteroclinic case in Fig. 21.

The pseudo-orbits obtained by applying the scattering maps σ_{ϵ}^1 or σ_{ϵ}^2 according to these rules are in fact the orbits of the mapping

(74)
$$T_{\epsilon}(I,\theta) := \begin{cases} \sigma_{\epsilon}^{1}(I,\theta), & \text{if } (I,\theta + \Delta^{1}(I)) \in \mathcal{S}_{1}, \\ \sigma_{\epsilon}^{2}(I,\theta), & \text{if } (I,\theta + \Delta^{2}(I)) \in \mathcal{S}_{2}, \\ \sigma_{\epsilon}^{2}(I,\theta) & \text{if } (I,\theta + \Delta^{2}(I)) \in \mathcal{S}_{3}, \\ \sigma_{\epsilon}^{1}(I,\theta) & \text{if } (I,\theta + \Delta^{1}(I)) \in \mathcal{S}_{4}, \\ \sigma_{\epsilon}^{1}(I,\theta) & \text{if } (I,\theta + \Delta^{1}(I)) \in \mathcal{S}_{5}. \end{cases}$$

There is another map \tilde{T}_{ϵ} , where in (74) we swap σ_{ϵ}^{1} with σ_{ϵ}^{2} . Then, applying \tilde{T}_{ϵ} has the opposite effect to applying T_{ϵ} .

Recall that in the proof of Proposition 5.7 we consider the set

$$X_{\epsilon} = \bigcup_{n \ge 0} T_{\epsilon}^{n}(\mathbb{A}'),$$

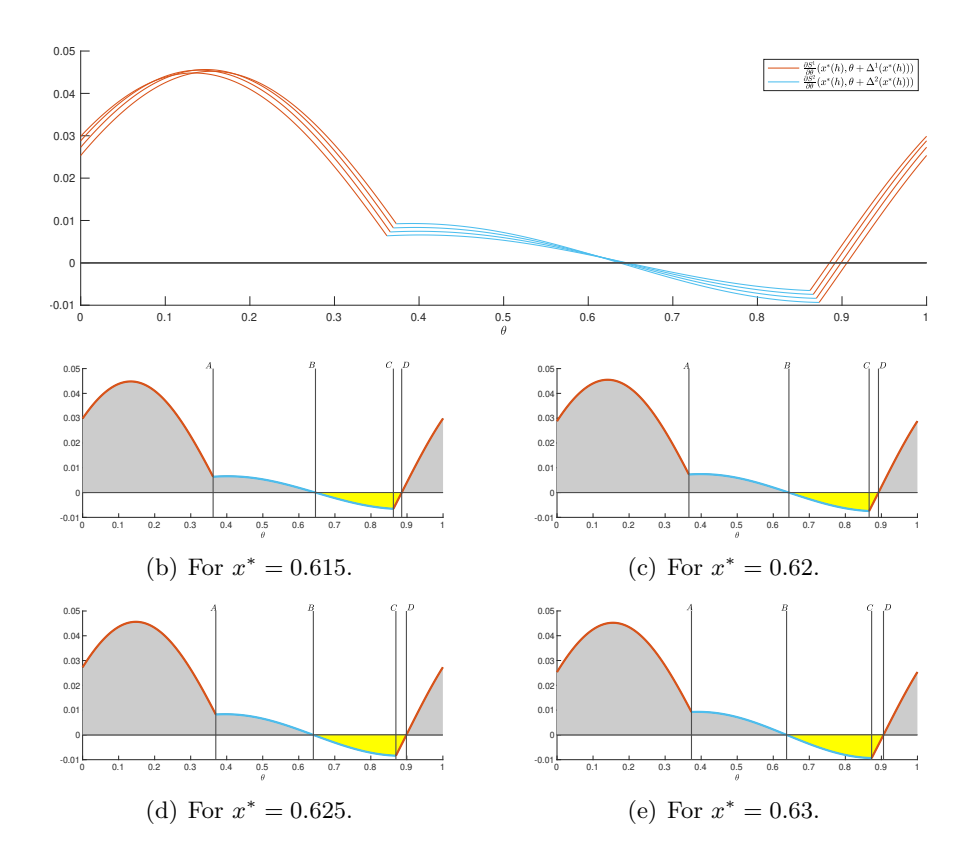


FIGURE 21. Heteroclinic connections.

where \mathbb{A}' is an annulus slightly smaller than and inside \mathbb{A} . If the set X_{ϵ} is not well-defined in \mathbb{A} there exist N such that

$$I_0 < I'_{\beta}$$
 and $I_N > I_{\beta}$ or $I_0 > I'_{\alpha}$ and $I_N < I_{\alpha}$.

In the first case we obtain an orbit of T_{ϵ} that grows the action coordinate from I'_{β} to I_{β} . In the second case, since \tilde{T}_{ϵ} has the opposite effect of T_{ϵ} , there is an orbit of \tilde{T}_{ϵ} that grows the action coordinate from I_{α} to I'_{α} . In either case we obtain a pseudo-orbit that increases the action coordinate by O(1).

If the set X_{ϵ} is a well-defined set in \mathbb{A} , then, as in the proof of Proposition 5.7, we apply Birkhoff's Ergodic Theorem. To obtain pseudo-orbits along which the action increases by O(1) we need to verify that there is a constant C>0 such that

(75)
$$\sum_{i=1}^{5} \int_{\mathcal{S}^{i}} \left[-\frac{\partial S^{\varsigma(i)}}{\partial \theta} (I, \theta + \Delta^{\varsigma(i)}(I)) \right] dI \wedge d\theta > C > 0$$

where $\varsigma(i) \in \{1,2\}$ is chosen by the rules described above.

x^*	$\int_0^A \frac{\partial S^1}{\partial \theta} d\theta$	$\int_A^B \frac{\partial S^2}{\partial \theta} d\theta$	$\int_{B}^{C} \frac{\partial S^2}{\partial \theta} d\theta$	$\int_{C}^{D} \frac{\partial S^{1}}{\partial \theta} d\theta$	$\int_{D}^{1} \frac{\partial S^{1}}{\partial \theta} d\theta$
0.615	0.01108517	0.00559062	-0.00569440	-0.00265228	0.00090362
0.62	0.01116304	0.00555252	-0.00596178	-0.00275864	0.00081121
0.625	0.01108579	0.00544458	-0.00623825	-0.00287422	0.00069592
0.63	0.01082731	0.00525498	-0.00654766	-0.00301109	0.00055637

Table 12. Integrals for the homoclinic case.

x^*	$\int_0^A \frac{\partial S^1}{\partial \theta} d\theta + \int_A^B \frac{\partial S^2}{\partial \theta} d\theta + \int_B^C \frac{\partial S^2}{\partial \theta} d\theta + \int_C^D \frac{\partial S^1}{\partial \theta} d\theta + \int_D^1 \frac{\partial S^1}{\partial \theta} d\theta$
0.615	0.00923273
0.62	0.00880635
0.625	0.00811382
0.63	0.00707991

Table 13. Sum of integrals for the homoclinic case.

x^*	$\int_0^A \frac{\partial S^1}{\partial \theta} d\theta$	$\int_A^B \frac{\partial S^2}{\partial \theta} d\theta$	$\int_{B}^{C} \frac{\partial S^2}{\partial \theta} d\theta$	$\int_{C}^{D} \frac{\partial S^{1}}{\partial \theta} d\theta$	$\int_D^1 \frac{\partial S^1}{\partial \theta} d\theta$
0.615	0.01240600	0.00128406	-0.00084456	-0.00007556	0.00179646
0.62	0.01277860	0.00140479	-0.00100277	-0.00009677	0.00162126
0.625	0.01299019	0.00151934	-0.00117848	-0.00012280	0.00143060
0.63	0.01302879	0.00162423	-0.00137258	-0.00015460	0.00122945

Table 14. Integrals for the heteroclinic case.

The corresponding integrals and their sums are given in the homoclinic case in the Tables 12 and 13, and in the heteroclinic case in Tables 14 and 15. In both cases, the sum of the integrals is positive. By Proposition 5.7 we obtain pseudo-orbits along which the action increases by O(1).

In order to obtain true diffusing orbits, we apply the shadowing lemma type of result [GdlLMS20, Theorem 3.7]. This result requires the inner dynamics given by f_{ϵ} restricted to the NHIM to satisfy Poincaré recurrence. Since we restrict ourselves to a bounded domain in \mathbb{A} , this condition is automatically satisfied. The aforementioned shadowing lemma implies that for any $\delta > 0$, any pseudo-orbit obtained by successively applying scattering maps according to the rules above can be shadowed by a true orbit.

Remark 6.1. Comparing the Tables 14 and 15, we note that the sum of the integrals is larger in the heteroclinic case in comparison to the homoclinic case, implying that this mechanism of diffusion by heteroclinic orbits is more efficient than the one by homoclinic orbits.

Still, both mechanisms of diffusion are not particularly efficient, since they involve applying scattering maps even when they yield energy loss. An alternative could be to apply only scattering maps that yield energy growth

x^*	$\int_{0}^{A} \frac{\partial S^{1}}{\partial \theta} d\theta + \int_{A}^{B} \frac{\partial S^{2}}{\partial \theta} d\theta + \int_{B}^{C} \frac{\partial S^{2}}{\partial \theta} d\theta + \int_{C}^{D} \frac{\partial S^{1}}{\partial \theta} d\theta + \int_{D}^{1} \frac{\partial S^{1}}{\partial \theta} d\theta$
0.615	0.01456639
0.62	0.0147051059
0.625	0.01463885
0.63	0.014355300

Table 15. Sum of integrals for the heteroclinic case.

in the domains where such scattering maps exist, and to apply the inner dynamics restricted to the NHIM in the domains where the scattering maps yield energy loss. However, for such a mechanism we would need detailed information on the inner dynamics.

References

- [AGMS23] Samuel W Akingbade, Marian Gidea, and Tere M-Seara. Arnold diffusion in a model of dissipative system. SIAM Journal on Applied Dynamical Systems, 22(3):1983–2023, 2023.
- [AP20] A.A. Ansari and S.N. Prasad. Generalized elliptic restricted four-body problem with variable mass. Astronomy Letters, 46:275–288, 2020.
- [Arn64] V.I. Arnold. Instability of dynamical systems with several degrees of freedom. Sov. Math. Doklady, 5:581–585, 1964.
- [BB13] Pierre Berger and Abed Bounemoura. A geometrical proof of the persistence of normally hyperbolic submanifolds. *Dynamical Systems*, 28(4):567–581, 2013.
- [Bel04] Edward Belbruno. Capture Dynamics and Chaotic Motions in Celestial Mechanics: With Applications to the Construction of Low Energy Transfers. Princeton University Press, 2004.
- [BG16] Jaime Burgos-García. Families of periodic orbits in the planar Hill's four-body problem. Astrophysics and Space Science, 361(11):1–21, 2016.
- [BGBFP22] Jaime Burgos-García, Abimael Bengochea, and Luis Franco-Pérez. The spatial Hill four-body problem I—An exploration of basic invariant sets. Communications in Nonlinear Science and Numerical Simulation, 108:106264, 2022.
- [BGCG⁺20] Jaime Burgos-García, Alessandra Celletti, Catalin Gales, Marian Gidea, and Wai-Ting Lam. Hill Four-Body Problem with Oblate Bodies: An Application to the Sun-Jupiter-Hektor-Skamandrios System. *Journal of Nonlinear Science*, pages 1–46, 2020.
- [BGD13a] J. Burgos-García and J. Delgado. On the "Blue sky catastrophe" termination in the restricted four body problem. Celestial Mechanics and Dynamical Astronomy, 117:113–136, 2013.
- [BGD13b] J. Burgos-García and J. Delgado. Periodic orbits in the restricted four-body problem with two equal masses. Astrophysics and Space Science, 345:247– 263, 2013.
- [BGG15] Jaime Burgos-García and Marian Gidea. Hill's approximation in a restricted four-body problem. Celestial Mechanics and Dynamical Astronomy, 122(2):117–141, 2015.
- [BGL23] Edward Belbruno, Marian Gidea, and Wai-Ting Lam. Regularization of the Hill four-body problem with oblate bodies. *Celestial Mechanics and Dynamical Astronomy*, 135(1):6, 2023.

- [BGLJ19] J. Burgos-García, J. Lessard, and J.D.M. James. Spatial periodic orbits in the equilateral circular restricted four-body problem: computer-assisted proofs of existence. Celestial Mechanics and Dynamical Astronomy, 131(2), 2019.
- [BLZ00] Peter W. Bates, Kening Lu, and Chongchun Zeng. Invariant foliations near normally hyperbolic invariant manifolds for semiflows. Trans. Amer. Math. Soc., 352(10):4641–4676, 2000.
- [Cap12] Maciej J. Capiński. Computer assisted existence proofs of Lyapunov orbits at L₂ and transversal intersections of invariant manifolds in the Jupiter–Sun PCR3BP. SIAM Journal on Applied Dynamical Systems, 11(4):1723–1753, 2012.
- [CFG22] Andrew Clarke, Jacques Fejoz, and Marcel Guardia. Why are inner planets not inclined? arXiv preprint arXiv:2210.11311, 2022.
- [CG23] Maciej J Capiński and Marian Gidea. Arnold diffusion, quantitative estimates, and stochastic behavior in the three-body problem. Communications on Pure and Applied Mathematics, 76(3):616–681, 2023.
- [CGDlL17] M. Capinski, M. Gidea, and R. De la Llave. Arnold diffusion in the planar elliptic restricted three-body problem: mechanism and numerical verification. Nonlinearity, 30(1):329–360, 2017.
- [CN19] A. Chakraborty and A. Narayan. A new version of restricted four body problem. *New Astronomy*, 70:43–50, 2019.
- [CPT22] S. Carletta, M. Pontani, and P. Teofilatto. Characterization of low-energy quasiperiodic orbits in the elliptic restricted 4-body problem with orbital resonance. *Aerospace*, 9:175, 2022.
- [DdlLS00] Amadeu Delshams, Rafael de la Llave, and Tere M. Seara. A geometric approach to the existence of orbits with unbounded energy in generic periodic perturbations by a potential of generic geodesic flows of \mathbf{T}^2 . Comm. Math. Phys., 209(2):353–392, 2000.
- [DdlLS06a] Amadeu Delshams, Rafael de la Llave, and Tere M. Seara. A geometric mechanism for diffusion in Hamiltonian systems overcoming the large gap problem: heuristics and rigorous verification on a model. *Mem. Amer. Math. Soc.*, 179(844):viii+141, 2006.
- [DdlLS06b] Amadeu Delshams, Rafael de la Llave, and Tere M. Seara. Orbits of unbounded energy in quasi-periodic perturbations of geodesic flows. Adv.~in Math.,~202(1):64-188,~2006.
- [DdlLS08] Amadeu Delshams, Rafael de la Llave, and Tere M. Seara. Geometric properties of the scattering map of a normally hyperbolic invariant manifold. Adv. Math., 217(3):1096-1153, 2008.
- [DGR] A. Delshams, M. Gidea, and P. Roldan. Accurate representation of the scattering map.
- [DGR16] Amadeu Delshams, Marian Gidea, and Pablo Roldan. Arnold's mechanism of diffusion in the spatial circular restricted three-body problem: A semi-analytical argument. *Physica D: Nonlinear Phenomena*, 334:29–48, 2016.
- [DKdlRS19] Amadeu Delshams, Vadim Kaloshin, Abraham de la Rosa, and Tere M Seara. Global instability in the restricted planar elliptic three body problem. Communications in Mathematical Physics, 366(3):1173–1228, 2019.
- [DS17] Amadeu Delshams and Rodrigo G Schaefer. Arnold diffusion for a complete family of perturbations. *Regular and Chaotic Dynamics*, 22(1):78–108, 2017.
- [DS18] Amadeu Delshams and Rodrigo G. Schaefer. Arnold diffusion for a complete family of perturbations with two independent harmonics. Discrete & Continuous Dynamical Systems A, 38(12):6047, 2018.
- [DSSY17] Suddhasattwa Das, Yoshitaka Saiki, Evelyn Sander, and James A Yorke. Quantitative quasiperiodicity. Nonlinearity, 30(11):4111, 2017.

- [DY18] Suddhasattwa Das and James A Yorke. Super convergence of ergodic averages for quasiperiodic orbits. *Nonlinearity*, 31(2):491, 2018.
- [E⁺13] Jaap Eldering et al. Normally hyperbolic invariant manifolds: the noncompact case, volume 2. Springer, 2013.
- [Fen72] Neil Fenichel. Persistence and smoothness of invariant manifolds for flows. Indiana Univ. Math. J., 21:193–226, 1971/1972.
- [FGKR16] Jacques Féjoz, Marcel Guardia, Vadim Kaloshin, and Pablo Roldán. Kirkwood gaps and diffusion along mean motion resonances in the restricted planar three-body problem. *Journal of the European Mathematical Society*, 18(10):2315–2403, 2016.
- [GdlL17] Marian Gidea and Rafael de la Llave. Perturbations of geodesic flows by recurrent dynamics. J. Eur. Math. Soc. (JEMS), 19(3):905–956, 2017.
- [GdlLM22] Marian Gidea, Rafael de la Llave, and Maxwell Musser. Melnikov method for non-conservative perturbations of the restricted three-body problem. Celestial Mechanics and Dynamical Astronomy, 134(1):1–42, 2022.
- [GdlLMS19] Marian Gidea, Rafael de la Llave, and Tere M Seara. A general mechanism of instability in hamiltonian systems: Skipping along a normally hyperbolic invariant manifold. *Discrete & Continuous Dynamical Systems-A*, 2019.
- [GdlLMS20] Marian Gidea, Rafael de la Llave, and Tere M-Seara. A general mechanism of diffusion in Hamiltonian systems: Qualitative results. Communications on Pure and Applied Mathematics, 73(1):150–209, 2020.
- [GM22] Marian Gidea and Jean-Pierre Marco. Diffusing orbits along chains of cylinders. Discrete and Continuous Dynamical Systems, 0:-, 2022.
- [GPS23] Marcel Guardia, Jaime Paradela, and Tere M Seara. A degenerate Arnold diffusion mechanism in the restricted 3 body problem. arXiv preprint arXiv:2302.06973, 2023.
- [Her79] M.-R. Herman. Sur la conjugaison différentiable des difféomorphismes du cercle à des rotations. *Inst. Hautes Études Sci. Publ. Math.*, (49):5–233, 1979.
- [HPS77] M.W. Hirsch, C.C. Pugh, and M. Shub. Invariant manifolds, volume 583 of Lecture Notes in Math. Springer-Verlag, Berlin, 1977.
- [KMWZ21] Tomasz Kapela, Marian Mrozek, Daniel Wilczak, and Piotr Zgliczyński. CAPD:: DynSys: a flexible C++ toolbox for rigorous numerical analysis of dynamical systems. Communications in nonlinear science and numerical simulation, 101:105578, 2021.
- [Kre78] Ulrich Krengel. On the speed of convergence in the ergodic theorem. *Monat-shefte für Mathematik*, 86(1):3–6, 1978.
- [Las90] J. Laskar. The chaotic motion of the solar system: A numerical estimate of the size of the chaotic zones. *Icarus*, 88(2):266–291, 1990.
- [LB22] R. Lara and A. Bengochea. A restricted four-body problem for the figure-eight choreography. *Regular and Chaotic Dynamics*, 26:222–235, 2022.
- [LG18] C. Liu and S. Gong. Hill stability of the satellite in the elliptic restricted four-body problem. *Astrophysics and Space Science*, 363:162, 2018.
- [MDCR⁺14] F. Marchis, J. Durech, J. Castillo-Rogez, F. Vachier, M. Cuk, J. Berthier, M.H. Wong, P. Kalas, G. Duchene, M.A. Van Dam, et al. The puzzling mutual orbit of the binary Trojan asteroid (624) Hektor. *The Astrophysical* journal letters, 783(2):L37, 2014.
- [Mey09] K. Meyer. Introduction to Hamiltonian Dynamical Systems and the N-body problem. Springer Verlag, 2009.
- [ML99] D.L. Maranhão and J. Llibre. Ejection-collision orbits and invariant punctured tori in a restricted four-body problem. *Celestial Mechanics and Dynamical Astronomy*, 71:11–14, 1999.
- [Mos58] Jürgen Moser. On the generalization of a theorem of A. Liapounoff. Communications on Pure and Applied Mathematics, 11(2):257–271, 1958.

JAIME BURGOS–GARCÍA, MARIAN GIDEA, AND CLAUDIO SIERPE

[RG06] Philippe Robutel and F Gabern. The resonant structure of Jupiter's Trojan asteroids—I. Long-term stability and diffusion. *Monthly Notices of the Royal Astronomical Society*, 372(4):1463–1482, 2006.

[Sze67] Victor Szebehely. Theory of orbits. The restricted problem of three bodies. New York: Academic Press, 1967.

FACULTAD DE CIENCIAS FÍSICO MATEMATICAS, UNIVERSIDAD AUTÓNOMA DE COAHUILA, UNIDAD CAMPO REDONDO, EDIFICIO A, 25020 SALTILLO, COAHUILA, MÉXICO *Email address*: jburgos@uadec.edu.mx

Yeshiva University, Department of Mathematical Sciences, New York, NY 10016, USA

Email address: Marian.Gidea@yu.edu

52

DEPARTMENT OF MATHEMATICS, SCIENCES FACULTY, UNIVERSITY OF BÍO-BÍO, CASILLA 5-C, CONCEPCIÓN, VIII-REGIÓN, CHILE Email address: csierpe@ubiobio.cl